Docking Control System for a 54-cm-Diameter AUV

Robert S. McEwen, *Member, IEEE*, Brett W. Hobson, *Member, IEEE*, Lance McBride, *Member, IEEE*, and James G. Bellingham, *Member, IEEE*

***Abstract*—The Monterey Bay Aquarium Research Institute (MBARI, Moss Landing, CA) has developed a 54-cm-diameter (21-in) docking AUV and companion docking station. This program resulted in four consecutive successful autonomous homing and docking events in the open ocean, which included downloading data, uploading a new mission plan, recharging the battery, and complete power cycling of the AUV. We describe the design, simulation, and at-sea test of the homing and docking control system.**

***Index Terms*—Autonomous underwater vehicle, docking, control system, mobile robot, sonar homing.**

I. Introduction

AUTONOMOUS underwater vehicles (AUVs) are playing a growing role in the ocean sciences. At Monterey Bay Aquarium Research Institute (MBARI, Moss Landing, CA), a 6-km-depth-rated mapping AUV is routinely generating bathymetry maps with unprecedented precision, resolution, and speed, and a second AUV routinely performs physical, chemical, and biological measurements in Monterey Bay. Both of these AUVs are characteristic of a class of vehicles carrying sophisticated, but power-intensive instrumentation. The high-power draw of the instrumentation limits today's AUVs to endurances of roughly one day. This means that for all but near-shore operations, the vehicles must be attended by a ship. As a consequence, the fundamental utility of the AUV is limited by ship support requirements. In some cases, the issue is cost. In other cases, the need for ship support makes activities impossible, for example, in high sea states, or when events cannot be predicted in advance for scheduling ship time.

Our docking station is designed to link to the power and communication infrastructure of a seafloor observatory, enabling the AUV to operate independently of a surface vessel for extended periods. In effect, the docking station allows the vehicle to connect to a mooring or a cabled instrumentation node. While docked, the AUV can recharge its batteries, download data, upload new instructions, and safely park until the next mission.

Manuscript received January 24, 2008; accepted August 21, 2008. This work was supported in part by the National Science Foundation under Grant NSF-OPP 9910290. Any opinions, findings, and conclusions or recommendations expressed in this material are those of the authors and do not necessarily reflect those of the National Science Foundation. This work was also supported by the David and Lucile Packard Foundation.

Associate Editor: L. Whitcomb.

R. S. McEwen, B. W. Hobson, J. G. Bellingham are with the Monterey Bay Aquarium Research Institute (MBARI), Moss Landing, CA 95039-9644 USA (e-mail: rob@mbari.org; hobson@mbari.org; jgb@mbari.org).

L. McBride was with the Monterey Bay Aquarium Research Institute (MBARI), Moss Landing, CA 95039-9644 USA (e-mail: lance.mcbride@ieee.org).

Color versions of one or more of the figures in this paper are available online at http://ieeexplore.ieee.org.

Digital Object Identifier 10.1109/JOE.2008.2005348

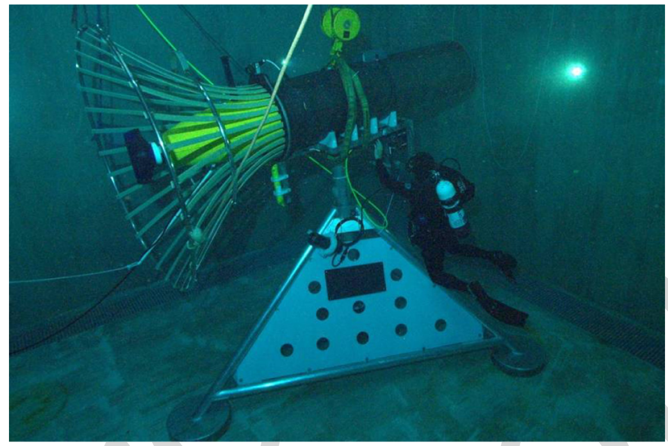

Fig. 1. AUV in the dock in a seawater test tank.

Once its batteries are recharged, the AUV can be deployed nearly instantaneously. Instead of being limited to studying static or repetitive subjects, the AUV can be dispatched on short notice to record episodic events such as canyon turbidity flows or plankton blooms, greatly increasing its scientific utility.

The move toward seafloor observatories is international in scope and creates the possibility that power and communication infrastructure will be available on the seafloor in a variety of interesting regions. At MBARI, the focus has been the development of the Monterey Accelerated Research System (MARS)-cabled observatory and the Monterey Ocean Observing System (MOOS) mooring-based observatory. MARS is a testbed for subsequent cabled observatories, and it provides an early opportunity to develop and demonstrate the AUV docking capability in a logistically benign environment. The compatibility of MARS and the docking system should ensure that the system is well suited to being deployed on future regional-scale cabled observatories (RCOs). The MOOS mooring system is also capable of supporting docking, and while MOOS is unable to supply as much power to a docking station as a shore-cabled observatory, it has the advantage of being much more easily relocated and deployed in regions of interest.

In the tests described below, the AUV was able to successfully dock and undock repeatedly in the open ocean, without assistance from the surface. Shore operators downloaded mission data and uploaded the next mission through an underwater Ethernet link, charged the battery, and completely powered the vehicle down and back up. Fig. 1 shows the dock and the vehicle in a test tank.

Fig. 2 shows the vehicle entering the dock in the Monterey Bay where the AUV was tested in a near-shore, disturbance-intensive environment. The dock worked well despite the fact that it was designed for a permanent deployment in a deeper,

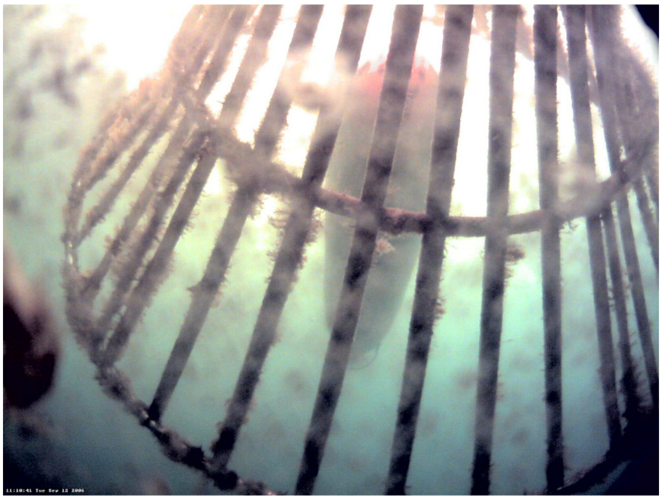

Fig. 2. AUV entering the dock in Monterey Bay.

more benign environment at the MARS-cabled observatory at 900-m depth in Monterey Bay. This deeper MARS site is free from surface wave motion and the intensive biofouling evident in Fig. 2.

II. Docking System Options

In past years, various research groups have developed different and innovative dock designs. Some of these require a hovering vehicle, such the intervention-style grappling system described in [1]. Another hovering vehicle has a tail hook and wire arrangement, where the vertical thrusters lower the vehicle into a cradle [2]. The designs of docks for flying vehicles, which rely on sustained forward motion for control, generally are either a pole or funnel type. In the pole design [3], the vehicle carries a latching mechanism that grabs on to a vertically moored pole or cable. In the funnel or cone design, the vehicle enters a circular funnel and is channeled into a tube where it is captured. There have been several designs of this type for smaller vehicles: the Remus/LEO15 system [4], [5], the Flying Plug [6], and the KRISO-KORDI [7]. To the best of our knowledge, there has never been a cone dock for a 54-cm-vehicle (21 in) that worked in the ocean.

We considered three classes of dock for MBARI's torpedo-like flying vehicle: the pole, the weathervaning cone, and the fixed cone. The pole is omnidirectional and eases the constraint on depth control, but requires the vehicle to carry an external, complex, motorized latching device. Establishing the power and data connection is difficult because the docked vehicle is not rigidly attached to the pole. A weathervaning cone is also omnidirectional, but securely captures the vehicle, making power and data connections easier. However, the dock must communicate its heading to the vehicle before docking, requiring a bidirectional communication system. This design must also transfer power and data across a moving interface, most likely using a slip ring. After considering these options, we chose the fixed cone primarily for its simplicity. Section IV describes the design in detail.

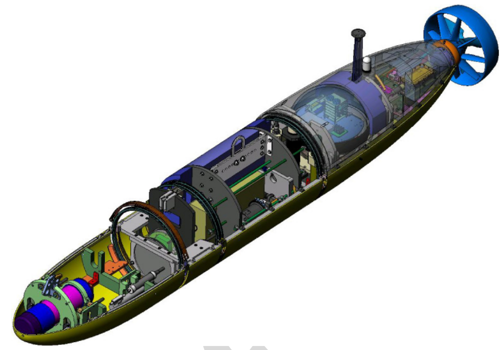

Fig. 3. Solid model of the docking AUV showing ultrashort base line (USBL) homing system as a cylinder in the bow.

III. The Autonomous Underwater Vehicle

The docking AUV is a Dorado/Bluefin 54-cm-diameter type (21 in), which has a Gertler body shape, series 58 model 4154, with a cylindrical midsection inserted at the point of maximum diameter, and a ring-wing tail [8], [9]. The vehicle is 358 cm long, and weighs 640 kg including entrained water. The vehicle has the capacity to carry three pressure-tolerant batteries, although during the short duration docking sea trials, it typically carried only one. Each battery provides 2 kWh of energy, giving a maximum range of approximately 70 km at 1.5 m/s with all three batteries present. The vehicle must maintain a minimum speed of approximately 0.8 m/s for controllability and to counteract the static buoyancy.

The ring-wing control and propulsion unit is shown in Fig. 3. A fractional horsepower direct current (dc) brushless motor with a 10 : 1 reduction gear box generates 52 N of thrust at 300 r/min. The ring wing is attached to a double-gimbal by eight equally spaced struts, which are small foils with a twist or preswirl. See Tables IV and V for numerical values, and [9] for a photograph and a mathematical model. Both the ring and the struts are based on a NACA ***[AU: Please define NACA]*** 0015 foil profile.

Gimbaling the ring and thruster together provide the control forces. At 3 kn, the lift from the ring is larger by about a factor of five than the lateral component of vectored thrust.

The control system consists of outer and inner proportional–integral–derivative (PID) loops for both heading and depth. The nominal horizontal-plane cross-track control loop is similar to the docking control presented in Fig. 8. A full explanation of the control system in both vertical and horizontal planes is in [9].

The vehicle navigation system is essentially Doppler velocity log (DVL)-aided dead reckoning, with periodic global positioning system (GPS) updates, which require surfacing. The expected accuracy is 4% of distance traveled (DT), circular error probability (CEP) with the navigation and control sampling rate of 5 Hz.

The AUV homes to the dock using an ultrashort base line (USBL) sonar transceiver mounted in the vehicle nose, as shown in Fig. 3. MBARI selected a Sonardyne-Scout-inverted USBL homing system, although other types of homing systems have been proven, such as an electromagnetic system [10] and optical systems [6] and [7]. The USBL has the advantage of much greater range and is also reliable, mature, and commercially available. The only drawback is that the Sonardyne Scout USBL selected is relatively large and takes up valuable space in the nose of the AUV. The USBL provides a bearing to its beacon in both the horizontal and vertical planes with a specified accuracy of 0.28° root mean square (RMS). The maximum sampling frequency of the USBL is 1 Hz due mostly to the beacon turnaround time and subsequent beacon lockout, which are 300 and 600 ms, respectively. Sonardyne reportedly is considering a faster beacon firmware design, which assumes a single, nearby vehicle. This sampling rate may go as high as 3 Hz.

The USBL is also useful as a general navigation instrument, because it provides position fixes much like GPS, but without surfacing or stopping. MBARI has already placed and surveyed over 100 USBL beacons in Monterey Bay, most of which are available for navigation.

IV. The Dock

The MBARI design approach keeps the dock as simple as possible and puts the complexity on the vehicle, because it is easier to retrieve the vehicle for maintenance. The dock is a benthic, fixed-heading cone with minimal moving parts and electronics. The cone design does not require the vehicle to carry an external latching mechanism, and also provides secure parking and a rigid data/power connection. The drawback is that the vehicle must fly with a near-bottom precision approach along a fixed flight path, possibly in a cross current, and must therefore contain the necessary electronics and algorithms.

The dock's entry is conically shaped, built of fiberglass staves held in place by two tubular stainless steel rings with an entrance diameter of 2 m. This entrance diameter was selected based on the following:

1) observations that the vehicle was passing well within two meters of the transponder during initial homing tests [11];
2) the predicted position deviation of the vehicle described in Section IX using the data from Section XI;
3) personal communications from local divers familiar with bottom currents in that area.

The dock body, consisting of the cone and the tube, is mounted on a 3-m-tall aluminum tripod (Fig. 1). The tube is made of fiberglass, and is of diameter 57 cm, 3 cm wider than the vehicle's diameter. An external pressure housing contains the electronics necessary to support power and data transfer between the vehicle and the cable. A USBL homing beacon is mounted below the front of the tube and is visible in Fig. 1. The small black cylinder at the top of the pyramidal base is a video camera, which turned out to be extremely useful for understanding dock/vehicle interaction dynamics and verifying missed distance measurements made by the USBL.

Although the dock body is fixed in heading, it gimbals in pitch and roll, due to a self-leveling pendulum designed for deployment on a sloped bottom at MARS. During ocean testing in relatively shallow water, described in Section X, the forces exerted by the short-period wave motion caused the dock to continually pitch up and down with an amplitude of approximately 10°–15°. This motion proved to be helpful in preventing the AUV from binding during entry. A next generation dock design will likely take more deliberate advantage of this pitching motion to prevent binding, as well as employing other aids such as mechanical rollers.

The vehicle is mechanically latched by a motorized peg that inserts into the AUV. We expect that a next generation design will reverse the peg and socket, placing the moving peg in the vehicle, in keeping with our design philosophy of an uncomplicated dock. Even with the peg located in the dock, the entire docking system has only a single drive motor and associated moving part.

The position of the vehicle in the dock is sensed by a pair of inductors: one mounted in the top of the vehicle, and the other fixed at a corresponding location in the docking tube. These have a range of several centimeters, and provide the trigger to raise the latching peg. These sensors were part of a docking module assembly that Florida Atlantic University (FAU, Boca Raton) developed under a grant from the U.S. Office of Naval Research (Arlington, VA) [12], and that we obtained from them. It is described further below.

V. Power and Data Transfer

Power transfer was accomplished by a transformer coil embedded in the tip of the latching peg and a corresponding coil in the socket. The system then transfers power inductively through the seawater without a metal-to-metal connection. The inductive power transfer subsystem was developed at FAU and was adapted for use on the Monterey Inner Shelf Observatory (MISO) cable where the sea trials were conducted. The adaptions included minor software modifications, and two Vicor dc : dc converters to convert from $+300\ V_{dc}$, coming in from the cable, to $+48\ V_{dc}$, required by the FAU module, and to $+12\ V_{dc}$ for the Ethernet wireless access points.

While deployed at sea, the power transfer was tested over a period of 10 min by charging the vehicle's battery. Measurements on shore showed 416 W delivered from shore, and measurements on the vehicle showed a total of 61.5 kJ were transferred into the battery. The efficiency of the inductive units was 77% with an overall power system efficiency of 48%. To improve the overall power system efficiency, the dock-side dc–dc converter would need to be redesigned to run directly off of the $300\ V_{dc}$ shore voltage.

The system is built so that the vehicle can be completely shut off while in the dock. The vehicle is restarted by applying power first to the vehicle's FAU inductive unit, which then provides power to the bus. After the vehicle's computer has booted, communications can then be reestablished between the computer and shore-side server by the wireless communications link. This power-saving feature was tested and verified at sea.

The AUV forms a wireless network link with the dock using modified off-the-shelf Ethernet antennas. One is embedded in the top of the vehicle, with its mate correspondingly located in the top of the docking tube. The static vehicle buoyancy holds the antennas nearly in contact, with the peg aligning the vehicle fore and aft. The link was developed to provide a 10 Mb/s data path across a 6.35-cm seawater gap. It is based on IEEE 802.11 and is fully compatible with the Ethernet network used throughout the vehicle and dock. The full specifications for the

TABLE I
DEPLOYED UNDERWATER WIRELESS SYSTEM PERFORMANCE SPECIFICATIONS

Protocol	802.11g
Transmission Frequency	2.4 GHz
RF Power	1 W
Antenna	0.22 λ_{air} whip
RF Link Margin	21.7 dB
Demonstrated seawater transmission distance	6.35 cm
Deployed seawater transmission distance	3.81 cm
ICMP transmission success rate	98.85%
Average ICMP time	4 ms
Bandwidth	9.5 Mb/s

link are shown in Table I. This system worked reliably during the sea trials.

VI. HOMING AND DOCKING SEQUENCE

The general homing and docking sequence consists of the following steps.

1) Locate and home to the dock. The vehicle uses its onboard navigation to transit within USBL range of the beacon, about 2 km. The USBL is directional with a ±85° field of view. The vehicle then homes to the dock using pure pursuit guidance, where the heading control system continuously points the vehicle at the beacon. This guidance strategy does not compensate for ocean current and thus the vehicle can be blown downwind while approaching. Pursuit guidance has the advantage of keeping the USBL pointed at the beacon for maximum signal strength.
2) Compute a position fix. When the USBL attains good signal strength, the vehicle uses its compass heading and the USBL bearing and range to compute a position fix. Based on previous testing, this occurs between 1000 and 200 m away from the dock. Because the homing control does not use compass heading or propagated position, a jump in the propagated position caused by the fix does not affect the vehicle control.
3) Fly to the start of the final approach path. The approach path is along the cone centerline, and begins about 300 m out. The approach may require the vehicle to turn away from the dock and temporarily lose USBL contact.
4) Execute final approach. The vehicle approaches along the cone centerline using a cross-track controller instead of pure pursuit. This means that the vehicle will track the approach path to the cone, and acquire a drift correction angle (crab angle) if the ocean current has a lateral component. This type of control uses both range and bearing from the USBL at 1 Hz, and uses the DVL and compass to dead-reckon between USBL updates. The vehicle slows to 1.0 m/s about 200 m from the dock. This allows time for the control loop to zero the cross-track error, and also prevents the vehicle from hitting the dock with too much force.
5) Latch. The vehicle uses the inductive position sensor and Ethernet contact to determine if it has fully entered. The algorithm then raises the peg and latches the vehicle.

The vehicle's automatic peg-raising code was not fully debugged at the time of the sea trials and worked sporadically in the preceding tank tests. During the sea trials, shore operators manually raised the pin by watching the vehicle enter the dock on camera. The Ethernet path from the main vehicle computer to the peg PIC passed through four wireless access points (WAPS), and we believe the source of the problems lay in the four routing tables.

Fig. 4 shows the various possibilities during the homing and docking sequence in state-diagram form. Step 1 of the enumerated list corresponds to the "homing" state in the figure, step 3 to "transit to outer marker," and step 4 to "docking." Items shown with an asterisk were planned but not implemented at the time of these tests.

The ability of the vehicle to sense a deceleration without network presence, that is, to sense that it is stuck either partially in the dock, or somewhere else, was not implemented for the sea trials, but is important and planned for later development. To account for this during the sea trials, we appended a time delay followed by a full reverse thrust behavior to the end of each mission. If the vehicle became stuck, it would run through the rest of the mission in place, but would end by reversing thrust, thus possibly freeing itself. In case the vehicle missed the dock, shore operators could simply terminate the mission over the radio modem after the vehicle surfaced but before the reverse thrust started.

The homing and docking states and associated control loops were tested separately. Homing was tested in fall 2005 in central Monterey Bay off Moss Landing. Docking was tested during summer and fall 2006 offshore Monterey Bay where the dock was attached to an underwater cable, as described in Section X.

The position fix update in step 2 was not implemented in time for the sea trials. However, it is straightforward and would eliminate surfacing the AUV for a GPS fix close to the dock, which would be impractical in the relatively deep water at the MARS location.

VII. UNDOCKING

The vehicle was designed to undock by lowering the peg and reversing the thruster. The vehicle is unstable in reverse, and therefore, thrusts with a fixed elevator angle and short duration. After the thruster shuts off, the vehicle floats up to a specified altitude that is above and clear of the dock. The vehicle then begins a normal mission with ahead thrust, which consists of a U-turn and a transit back to the outer waypoint.

During the sea trials, the shore operators manually lowered the peg and initiated the undocking mission while watching on the camera, because the vehicle's onboard peg control code was not yet reliable.

A planned, but not implemented feature, was an undocking behavior that would pulse the thruster forward and backward to break loose if the vehicle had difficulty backing out. Should the vehicle become permanently stuck, the final dock design would contain an acoustic release at the top of the base, and the rest of the dock would be positively buoyant. A support ship could then trigger the release and recover both the vehicle and the dock.

VIII. HOMING CONTROL LOOP

This section explains the homing control loop that operates in step 1 (Section VI). Section IX explains the docking control loop of step 4.

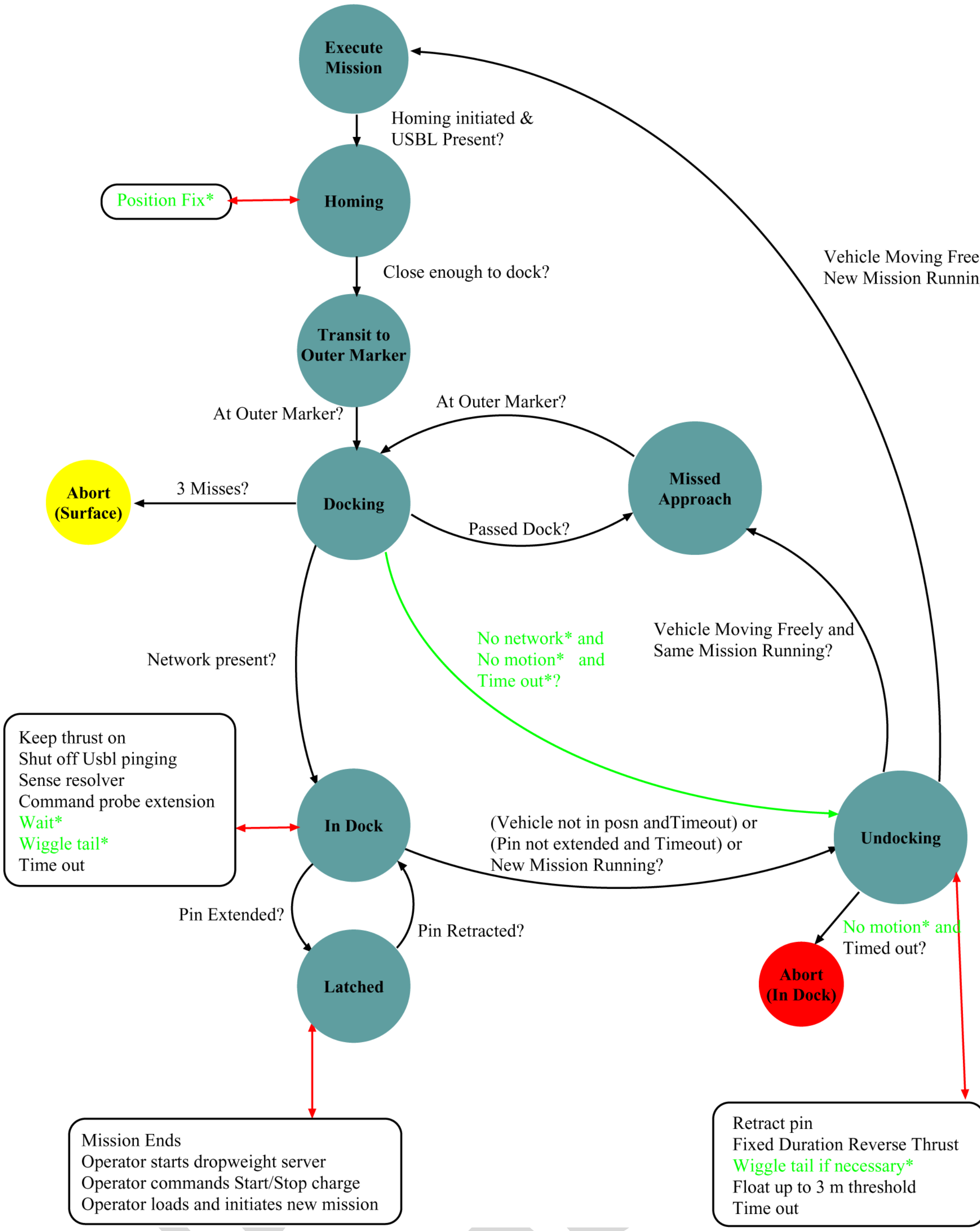

Fig. 4. State diagram of the mission, homing, and docking sequence. An asterisk indicates a planned item, not yet implemented during sea trials.

Fig. 5 shows angle and reference frame definitions used in the following homing analysis. Angles are defined to be positive clockwise.

The design and analysis of the homing and docking control loops are fundamentally based on the dynamics of the vehicle, described by coupled nonlinear equations of motion (EOM) such as those in [13]. The vehicle travels in straight and level flight when approaching the dock, with small angular and translational deviations, in which case the horizontal-plane and vertical-plane dynamics decouple. Equation (1), shown at the top of the next page, is the horizontal-plane, or sway-yaw dynamics linearized about straight and level flight. It is fourth order and consists of $\Delta\psi$, heading deviation; y, cross-track displacement; v, lateral velocity component in the body frame; and finally, r, which is heading rate. See [14, p. 117] and [9] for derivations. Tables II–VI in the Appendix define the symbols and numerical values of the constants.

The depth control did not require any special modifications for docking, and so discussion of the vertical-plane dynamics and control [9] are not repeated here.

The origin of body-fixed coordinate system assumed by (1), and the values in Tables II and III, is amidships, that is, along

$$\begin{bmatrix} m - Y_{\dot v} & mx_G - Y_{\dot r} & 0 & 0 \\ mx_G - N_{\dot v} & I_{zz} - N_{\dot r} & 0 & 0 \\ 0 & 0 & 1 & 0 \\ 0 & 0 & 0 & 1 \end{bmatrix} \begin{bmatrix} \dot v \\ \dot r \\ \dot y \\ \Delta\dot\psi \end{bmatrix}$$
$$= \begin{bmatrix} (Y_v - Y_{\mathrm{RF}} - Y_A)U & (Y_r - m - x_R Y_{\mathrm{RF}} - x_A Y_A)U & 0 & 0 \\ (N_v - x_R Y_{\mathrm{RF}} - x_A Y_A)U & (N_r - mx_G - x_R^2 Y_{\mathrm{RF}} - x_A^2 Y_A)U & 0 & 0 \\ 1 & 0 & 0 & U \\ 0 & 1 & 0 & 0 \end{bmatrix} \begin{bmatrix} v \\ r \\ y \\ \Delta\psi \end{bmatrix}$$
$$+ \begin{bmatrix} Y_R U^2 + T_P \\ (Y_R U^2 + T_P)x_R \\ 0 \\ 0 \end{bmatrix} \delta_R - \begin{bmatrix} (Y_v - Y_{\mathrm{RF}} - Y_A)U \\ (N_v - x_R Y_{\mathrm{RF}} - x_A Y_A)U \\ 1 \\ 0 \end{bmatrix} v_c \qquad (1)$$

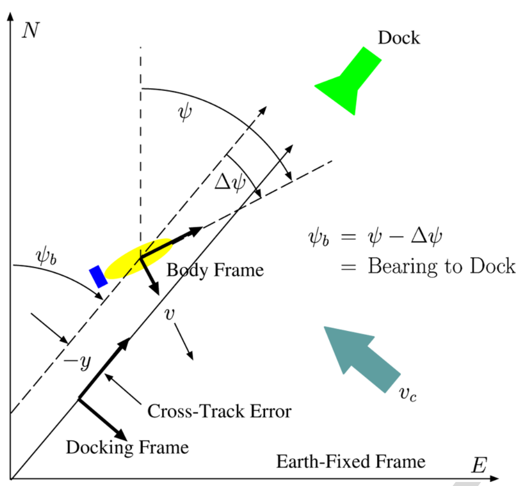

Fig. 5. Angle and reference frame definitions: y is the lateral displacement of the vehicle from the dock centerline, $\Delta\psi$ is the dock-relative heading, and v_c is cross current.

the centerline at half the overall length. It is *not* at the center of mass or the center of buoyancy.

Although the control surface is a double-gimbaled ring wing, small motion about the vertical axle is termed "rudder motion," and "elevator motion" is about the horizontal axle. In (1), Y_{RF} is the sway force coefficient due to the ring fixed in the neutral position

$$Y_{\mathrm{RF}} = \frac{1}{2}\rho A(C_{L\alpha} + C_{Do}) + \frac{1}{2}\rho A_S(C_{SL\alpha} + C_{SDo}). \qquad (2)$$

Here the subscript RF denotes rudder fixed.

A is the area of the ring, defined as chord × diameter, that is

$$A = \bar c_R d_R. \qquad (3)$$

A_S is the equivalent strut area, defined to be

$$A_S = 2(1 + \sqrt{2})\bar c_S b_S. \qquad (4)$$

$C_{L\alpha}$ is the slope of the coefficient of lift of the ring, and C_{Do} is the coefficient of drag. Similar symbols with subscripts S and F refer to the struts and RF/GPS fin, respectively. It is common to subsume the rudder-fixed portion of the force Y_{RF} into the stability derivatives. In this presentation, Y_{RF} is added explicitly in (1), and so the stability derivative values in Table III are for the fuselage only.

Y_A is the sway force due to the RF/GPS antenna fin

$$Y_A = \frac{1}{2}\rho A_F(C_{FL\alpha} + C_{FDo}) \qquad (5)$$

where A_F is the area. Fig. 1 shows the fin.

Y_R is the sway force coefficient due to a deflected rudder

$$Y_R = \frac{1}{2}\rho A C_{L\alpha}. \qquad (6)$$

v_c is cross current, modeled as a disturbance input, and it is shown in Fig. 5.

The homing control loop implements pure pursuit guidance, which requires that the vehicle's nose continuously point at the beacon during the approach. Pure pursuit is a special case of the well-known proportional navigation technique used for missile guidance [15]. Pure pursuit is proportional navigation with a gain of unity. Larger gains will cause the pursuing vehicle to lead the target and intercept faster, but the algorithm is more complicated. Proportional navigation is unnecessary in our case because the time-to-intercept is unimportant, and also because the vehicle does not come directly into the dock, but must first transit over to a fixed approach path after it gets to ***[AU: "gets to" what? Is something missing here?]*** with several hundred meters. The dock has a fixed heading and the vehicle must line up with it, much like an airplane approaching a runway.

When the homing loop is first initiated, it uses cross-track waypoint control to fly toward a preprogrammed dock location until the USBL receives a response from the beacon. From that point on, the algorithm latches the beacon location, and flies towards that point until the USBL updates with a new location. Updates occur every one to three seconds depending on range.

Fig. 6 shows the homing control loop. It is multirate PID with the option for feedback on the lateral speed state v. The lateral speed feedback term was not used in the final design. The cross-track state y and compass heading state ψ are unnecessary for homing and are, therefore, uncontrolled and ignored.

The reference input $\Delta\psi_R$ represents the angular motion of the dock relative to the vehicle. If the AUV is being carried laterally by current, the body-referenced heading to the dock changes. Thus, this control loop needs to be able to track at low frequencies. An integrator was included in the controller

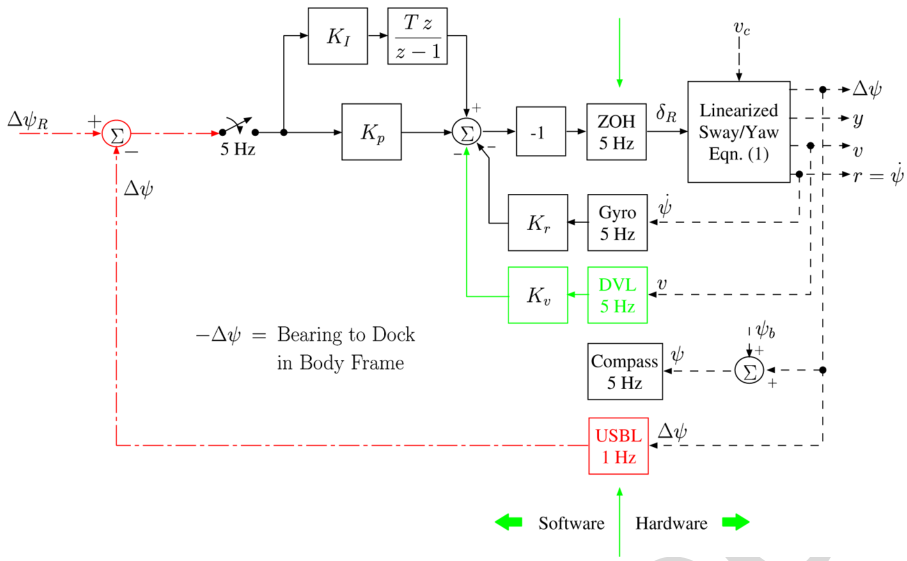

Fig. 6. Pure-pursuit homing control loop. The outer USBL loop is shown with short and long dashes because it has a sampling rate between 1 and 3 Hz, depending on the distance of the vehicle from the beacon. The rest of the system is at 5 Hz. The dashed lines indicate natural connections. The K_v rate gain was found in practice to be unnecessary and set to zero. Tables II–VI furnish the parameter values.

to give a total of two free integrators, counting the one in the plant where $\dot{\Delta\psi} = r$, as shown by (1). This closed-loop system will track constant angular motion (a ramp) with no steady-state error. Additionally, the steady-state step response to a lateral current has zero error.

A constant lateral current will cause the homing loop continuously to turn the vehicle so that as seen from above, the vehicle spirals in toward the dock. In an extreme case, the vehicle will end up approaching from down wind. Pure pursuit has the advantage of keeping the beacon centered in the USBL field of view for maximum signal strength while the vehicle gets close.

Fig. 7 shows the heading response to a $v_c = 25$ cm/s lateral current step, determined by simulation using (1). Assuming that the vehicle is at least 200 m from the dock, this heading error is insignificant because the control loop has ample time to recover. $v_c = 25$ cm/s was the maximum constant cross current expected at the test site in nonstorm conditions, and is discussed further in Section XI.

In addition to displacing the vehicle, a lateral current step exerts a yaw torque due to the lever arm between the center of pressure and the center of mass. Equation (1) models this, as shown by the N_v term in the disturbance (v_c) input matrix.

The dotted curve shows the response assuming the outer USBL loop has a sampling period of 3 s, which it does at the outer limit of its range. The inner gyro feedback loop still runs at 5 Hz. As the vehicle approaches, the USBL sampling period drops to 1 s. Fig. 7 shows that the slow outer loop does not significantly degrade the performance.

Between USBL sample periods, the 5-Hz heading loop maintains the last bearing determined by the USBL and the compass.

The control gains were empirically chosen and resulted in a dominant pole pair with a damping of 0.77 and a time constant of 17 s. This means that the vehicle will travel about 75 m before transients induced from step disturbances die out. Because we expect this loop to be in operation from 1 to 2 km out, these time constants are acceptable. Gain values are in Table VII.

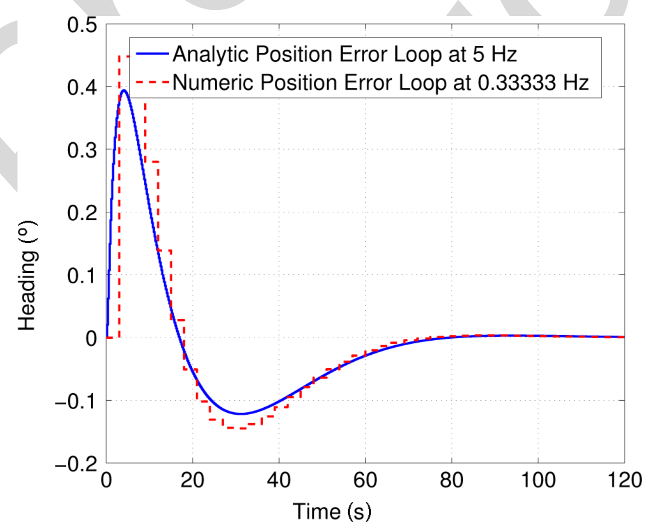

Fig. 7. Simulated closed-loop heading response to a 25-cm/s lateral step current using the control in Fig. 6.

The eigenvalues were determined by substituting analytically determined stability-derivative values into (1) and combining the result with the control loop shown in Fig. 6. Numerical values are shown in Tables II–VI.

IX. Docking Control Loop

Fig. 8 shows the docking control loop. It differs from the homing control loop because now the cross-track error state is computed from the USBL and fed back. The vehicle will now fly down a fixed approach path and will not be blown downwind by ocean currents. The integrator, which has now been moved to cross-track error, will crab the vehicle so as to keep the cross-track error at zero, should there be a cross current.

In Fig. 8, there is a smoothing filter after the waypoint control, which has a time constant of 2.5 s. This filter was neglected in

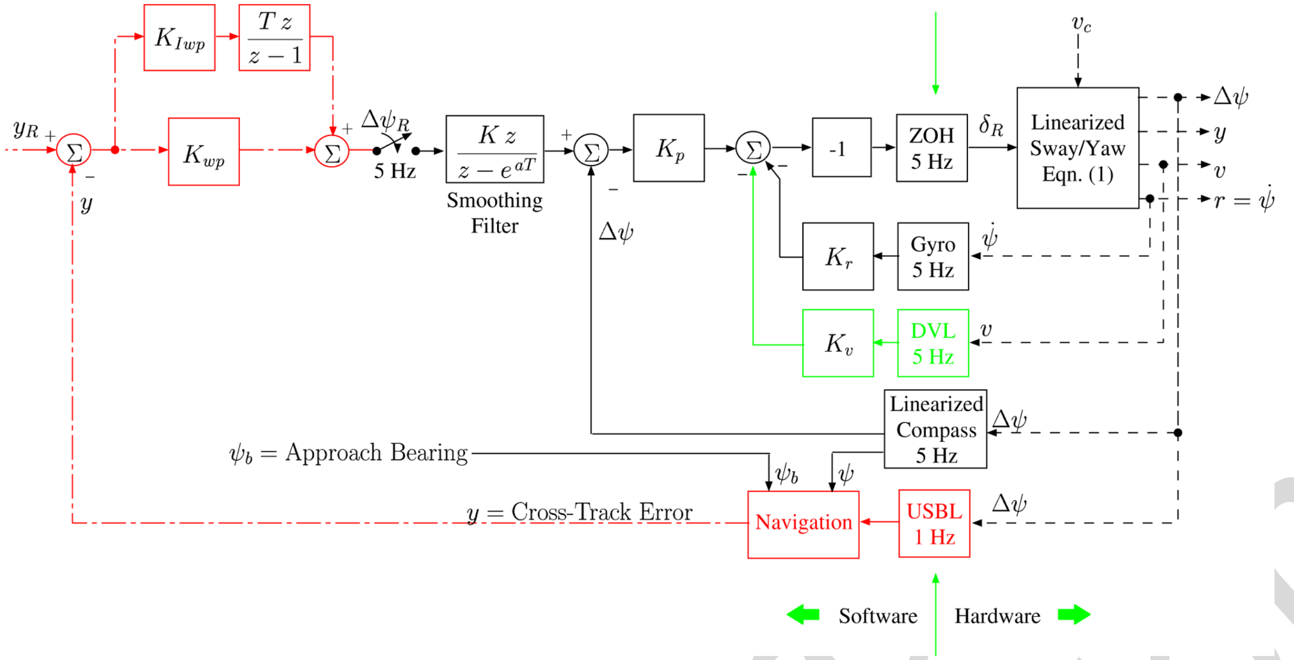

Fig. 8. Cross-track docking control loop. This system does not switch on until 200 m from the beacon. Consequently, the outer USBL loop, shown with long and short dashes, runs at about 1 Hz, as opposed to the pure pursuit system in Fig. 6, where the vehicle may be as far as 2 km away when it acquires the beacon.

the analysis below because it is much faster than the slowest roots of the closed-loop characteristic equation.

Because the vehicle position is now computed from the USBL, the navigation is free from the accruing odometry error inherent in dead reckoning. The measurement error of the USBL is proportional to the range, and thus decreases as the vehicle closes on the dock. This is fundamentally what makes the docking system work and is the reason for having a homing system.

The heading of the dock ψ_b was measured after deployment and is a known constant. It is used inside the USBL feedback loop to convert heading deviation to cross-track error.

As in the case of the homing controller, this control has a fall back in case the USBL drops out. It latches the last dock position measured by the USBL and continues by DVL-aided dead reckoning.

Control gains were again empirically determined, with K_v kept at zero. Values are shown in Table VIII. The cross-track error step response is dominated by a closed-loop pole pair with damping 0.29 and a time constant of 55 s. Fig. 9 shows simulated cross-track error response to a-25 cm/s current step.

Although the transients damp slowly, the error is well below the 1-m dock aperture radius after 100 s, while the vehicle has 100 m yet to travel before encountering the dock. This assumes that the docking control is initiated 200 m from the dock on the approach path, and the vehicle has also slowed to 1.0 m/s. The thrust is also reduced to 22 N. These two values were used in (1) along with the gains in Table VIII to produce Figs. 9 and 10.

In addition to crabbing into a constant tidal cross current, the control loop must perform in the presence of 8–12-s wave motion. The green curves in Fig. 10 show the steady-state sinusoidal response of cross-track error to lateral current. The frequency region bounded by the vertical magenta lines rep-

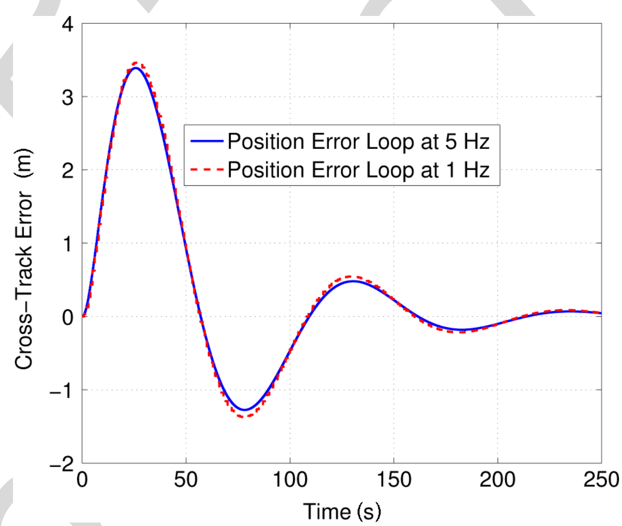

Fig. 9. Simulated closed-loop cross-track error response to a 25-cm/s lateral step current using the control in Fig. 8.

resents the wave energy. ***[AU: In many places in the paper you mention color. Please rewrite so that color is not mentioned. The figures will be published in b/w in print and in color online.]*** The black curve is the open-loop transfer function, which is coincident with the closed-loop transfer function in the region of the wave energy, showing that the control loop has rolled off there and has no effect. At the low end of the wave spectrum, the closed-loop gain is a factor of 2.5, and it decreases to less than one at the high end. Typically, the wave period is close to 10 s, where the loop gain is near unity, implying that a 30-cm/s wave motion will deviate the vehicle less than 30 cm from the flight path. Close examination of ADCP ***[AU:***

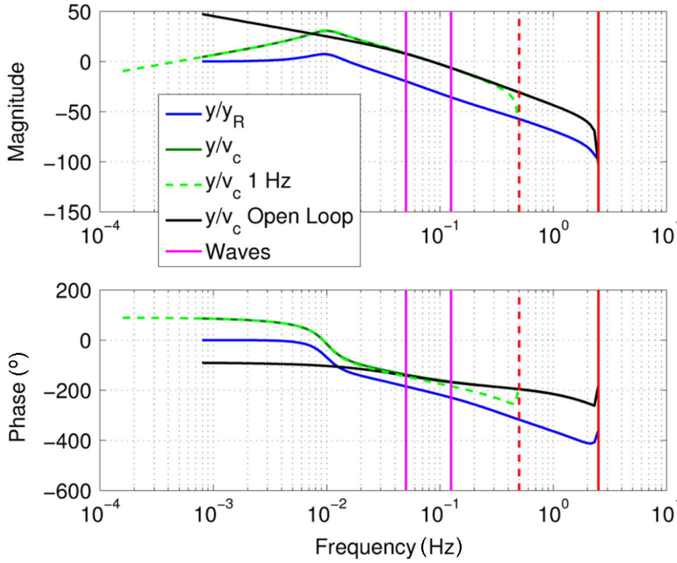

Fig. 10. Bode plot of cross-track docking control loops shown in Fig. 8.

Please define ADPC]data taken during the docking trials showed that the wave period was 9.3 s with 3σ amplitude of about 30 cm/s. This data is summarized in Fig. 15.

The dashed green curves in Fig. 10 show the multirate transfer function with the outer USBL loop at 1 Hz, and the other loops at 5 Hz. The solid green curves show the best case for comparison, where the USBL loop is assumed to run at 5 Hz. The 1-Hz sampling does not appreciably degrade the performance. The dashed vertical red line shows the Nyquist frequency for the 1-Hz/5 Hz multirate system and the solid line for the 5-Hz monorate.

X. Sea-Trial Results

The MBARI team conducted the first at-sea homing trials on December 11, 2005, offshore Moss Landing, CA, which is north of Monterey. The test area had a flat bottom about 15 m deep, without any nearby obstructions or kelp beds. The transponder was moored about 5 m off the bottom. The vehicle was acquiring the transponder at distances exceeding 2 km and homing to within 50 cm. See [11] for details.

Docking was tested separately from homing, during summer and fall 2006 at the MISO, operated by Naval Postgraduate School (NPS, Monterey, CA) [16] and Associate Professor T. Stanton, who generously allowed MBARI full access to the facility. MISO is a cabled facility that provides power and Ethernet 600 m offshore, in 12 m of water. The shallow depth makes this site subject to 9–12-s short-period wave motion, as well as 12-h tidal currents. The observatory has an upward-looking ADCP, and NPS maintains an archive of water-current measurements stretching back for many years.

The docking flight pattern was a rectangle of 300×50 m^2, oriented with the long sides perpendicular to the shore. The approach to the dock at MISO was a corridor about 150 m wide, defined by kelp beds on either side, with the flight pattern running through this corridor. Docking tests began with the vehicle at the outer end of the rectangle, 300 m from the dock, where it

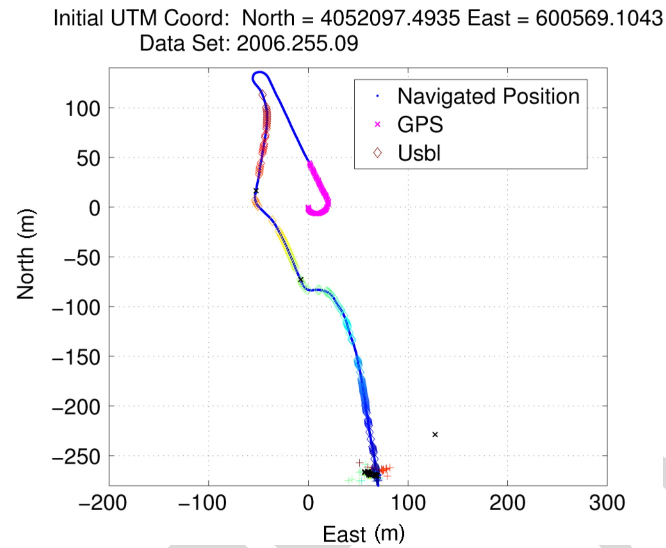

Fig. 11. Vehicle track during a docking trial. The + points are USBL measurements of the dock location. The diamonds show the vehicle's location when it took the measurement. Fig. 12 shows an enlargement of the point cluster at the bottom.

would get a GPS fix. The vehicle then submerged and proceeded towards the outer marker waypoint, 200 m from the dock. At the outer marker, it slowed to 1.0 m/s and transitioned to the docking control state shown in Fig. 4, with the cross-track control loop shown in Fig. 8.

The USBL performed well during the 2005 homing trials, with little noise and few dropouts, leading us to conclude that little filtering was necessary. However, the noise environment at the MISO docking site was worse, due perhaps to the proximity of the shoreline, the surf, and nearby kelp beds.

The noisy USBL data at MISO was significant in that it was causing the vehicle to consistently miss the dock by 3–10 m. This led to the design of a moving-window median filter that proved to be very effective. The vehicle made the first controlled dock after implementing the filter and successfully docked on every attempt thereafter. There were four consecutive dockings.

A median filter can be effective for sonar applications because it rejects multipath, as long as there are fewer measurements corrupted by multipath than the uncorrupted ones.

Before median filtering, the USBL measurements were passed through simple outlier rejection tests. The data had to pass all of the following to be considered valid:

1) there must be a preset number of good consecutive samples;
2) the vehicle must not be turning too fast;
3) the measured bearing must not be too great.

These tests are not switched on until the vehicle is near enough to the transponder that the signal is strong.

The median filter then consists of taking the last 11 valid USBL measurements and computing the median of each axis individually. The navigation first converts the measurements to UTM***[AU: Please define UTM]*** locations, so that each measurement appears as a fixed location on a map, such as those in Figs. 11 and 12. Median filtering the eastings and

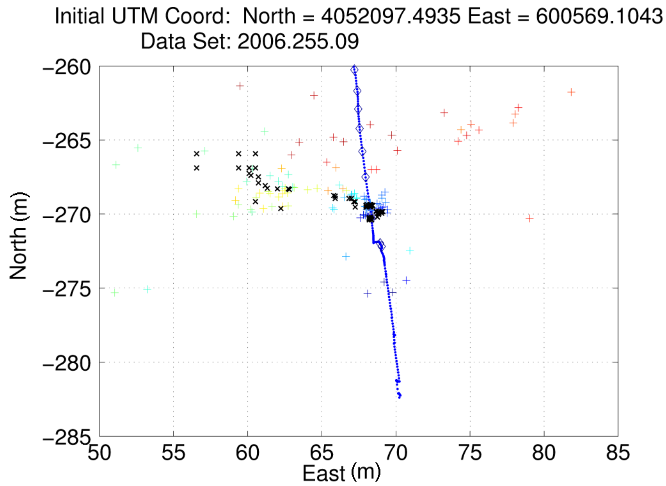

Fig. 12. Enlargement of the USBL dock hits. The $+$'s are raw data, and the x's are the filtered result. The colors of the $+$'s correspond to the diamonds in the preceding figure.

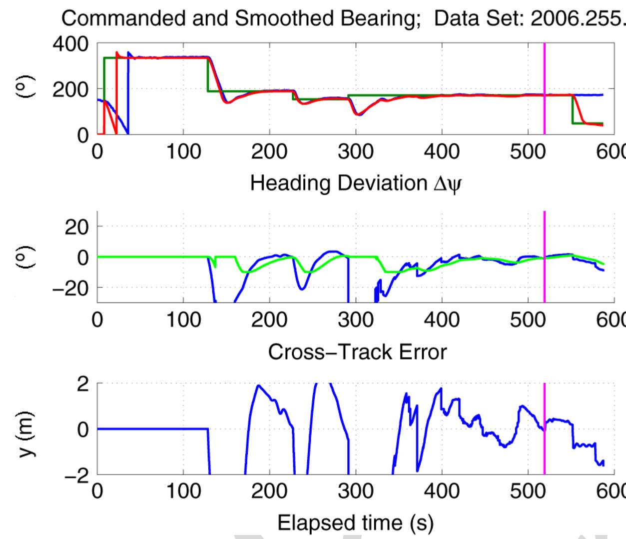

Fig. 13. Cross-track error, heading deviation, and heading during the docking event.

northings separately has the interesting effect of producing a location that is not the same as any of the measurements, yet it is contained within the largest cluster.

Fig. 11 shows the vehicle path, as seen from above, of the second docking mission. The axes are eastings and northings (UTM) in meters. The magenta points at the start, near (0,0), are GPS hits. The vehicle submerges, turns, and flies north to the first waypoint, then turns again to the south and passes through two more waypoints. The third waypoint is the outer marker where the vehicle transitions to docking control. The color-coded diamonds overlaying the path show the location of the vehicle at each USBL measurement. The color shows the distance from the transponder and corresponds to the color of the measured location indicated by a $+$. Black $\times$'s show the location of filtered points.

Fig. 12 shows a zoom of the dock location in Fig. 11. There is a distinct cluster of points about 8 m to the west of the dock, detected by the USBL when the vehicle was around 200 m out. The error is presumed to be due to a bounce (multipath). This cluster contains many valid hits. As the vehicle closes, however, this cluster is discarded by the moving window and the valid hits then cluster at the dock, precisely as desired.

Operators viewing the vehicle entering the dock on the video camera judged the position error to be between 5 and 10 cm, well under a vehicle diameter.

The jog after the third waypoint, at $(0, -70)$, is caused by the initiation of the docking control loop. It turns the vehicle to the east to bring it onto the fixed flight path heading of $\psi_b = 171^\circ$. From that point in, the cross-track error is computed directly from USBL measurements, and not from propagated position.

The top strip of Fig. 13 shows yaw commands during the approach to the dock. The green line is commanded bearing to each of the three waypoints, followed by a flight path approach of 171°, beginning at 291 s. The approach bearing is labeled ψ_b in Fig. 8. The red line in Fig. 13 is the filtered heading command, and the blue is the measured. They correspond to $\psi_R = \Delta\psi_R + \psi_b$ and $\psi = \Delta\psi + \psi_b$, respectively. The commands to turn the vehicle from each waypoint to the next are clearly visible at 128 and 227 s, with ψ tracking as expected. The maneuver at 291 s is interesting, where ψ_R increases, but the vehicle commanded heading appears to turn in the opposite direction. This is because the docking controller has activated and must now slew the vehicle not only onto the specified bearing of $\psi_b = 171^\circ$, but must do so on the approach path. To do this, the docking controller must first turn the vehicle in the opposite direction to get onto the line, before turning back to the specified bearing.

The middle strip of Fig. 13 shows heading deviation $\Delta\psi$, which corresponds directly with the same symbol in Fig. 8. The green curve is the crab angle, commanded by the integrator. It is apparent that there is little cross current during this approach, since the crab angle approaches zero as the control reaches steady state just before each of the two waypoint changes.

The character of the blue $\Delta\psi$ curve changes when the waypoint control activates at 291 s. This is because the cross-track error was previously computed from the propagated position, determined from DVL-aided dead reckoning. After 291 s, the cross-track error is computed from the filtered USBL measurements and the compass. Several jumps in heading deviation are apparent between 320 and 450 s due to USBL noise.

The bottom strip shows the cross-track error. It is converging to under a meter after 400 s. Interestingly, the USBL apparently got some hits that took the vehicle almost a meter off track at 490 s, but then the measurements improved until the vehicle had zero measured cross-track error only about 4 s before contact. The measured error at the moment of contact, at 519 s, was 10 cm, slightly larger than what was apparent in the video.

There were three additional docking events, each appearing much like this one, indicating that the docking control is repeatable, at least in the cross-current conditions shown in Fig. 15.

Depth control is unchanged from the standard algorithm as described in [9]. The vehicle flew at 12-m depth during its final approach, until about 50 m out, where it transitioned to a 3-m altitude track. The dock is located on a slight slope and is 3 m high in 12 m of water.

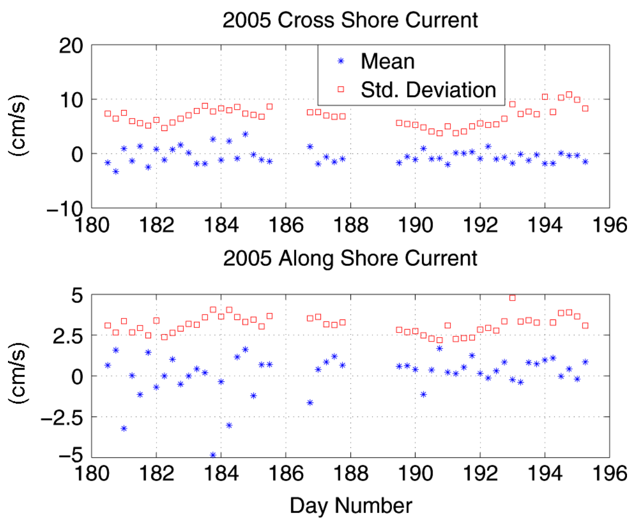

Fig. 14. Six-hour current statistics at 1.8-m altitude. Ten-second wave motion is averaged out.

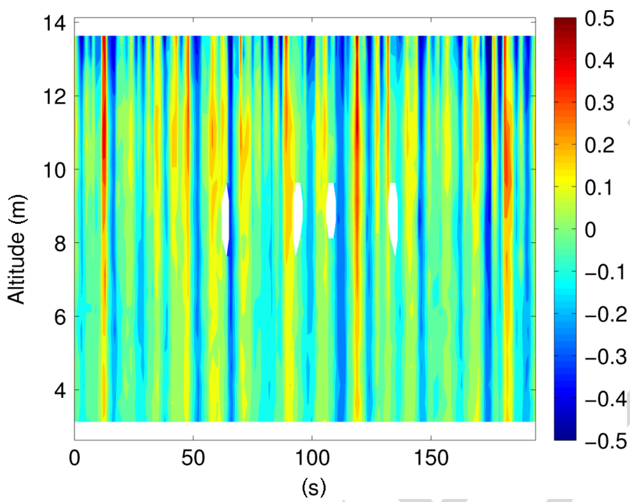

Fig. 15. Along-shore current as a function of altitude at MISO on the moment of the docking event in Figs. 11–13, September 12, 2006 (day 255), 19:36:00 Z. The colorbar shows meters per second.

XI. Dock Test Environment

Fig. 14 shows statistics of cross-shore and along-shore tidal currents at the MISO docking test site during July and August 2005, which is a representative period for the docking trials. The measurements are at 1.8-m altitude. The along-shore current is of primary concern because it is perpendicular to the approach path and will tend to carry the vehicle off track. The vehicle approach altitude was 3 m, where the current was expected to be larger, and so the design had to allow for currents greater than shown.

Blue points are the mean current over a 6-h period, which shows the tidal component with wave motion averaged out. The sampling period was between 1 and 2 s. Tidal currents act as a constant during a docking approach because an approach takes only a few minutes.

The standard deviation of the along-shore tidal component is 3.8 cm/s, with a maximum surpassing 5 cm/s. The constant-current design specification was consequently taken to be 25 cm/s, keeping in mind that the currents tend to be faster further above the sea bed, and allowing a margin. High-frequency ADCP data, such as that shown in Fig. 15, was not obtained in time for the control design, and so the design is based primarily on the data in Fig. 14.

Fig. 15 shows a 3-min segment of the full 1-s data set of along-shore current measurements, taken on the day that the AUV docked. At meters altitude, the tidal (average) current was 2.0 cm/s to the north, with a 9.3-s wave component, with standard amplitude deviation of $\sigma = 9.4$ cm/s.

The figure shows that the short-period wave current tends to increase with altitude, justifying a design margin for current greater than what was measured at 1.8 m in Fig. 14.

XII. Conclusion

A prototype AUV docking system has been designed, built, and tested at sea. The dock was attached to the MISO cabled observatory in southern Monterey Bay, and used to support docking operations with a Dorado 54-cm-diameter (21 in) AUV. All of the capabilities required for a docking capability for seafloor observatories have been demonstrated, including the following:

1) homing and capture of the AUV in the docking station;
2) establishing an Ethernet connection between the vehicle and the dock using a short-range radio frequency communication system;
3) complete interactivity with the vehicle including recovering mission data to shore, downloading new missions to the vehicle, and even adding new code to the vehicle and compiling *in situ*;
4) inductive transmitting power to the vehicle;
5) charging vehicle batteries from observatory power;
6) turning the vehicle off, and then waking it up from the dock;
7) undocking the vehicle from the dock and commencing missions.

Appendix

See Tables II–VI.

TABLE II
General Parameters and Mass Properties in (1)–(6) for the Homing Control

m	640.3	kg	Mass
I_{zz}	475.0	kg-m^2	Inertia
x_G	0.119	m	CG offset
x_R	-1.79	m	Dist. to rudder
x_A	-1.03	m	Dist. to antenna
U	1.54	m/s	Speed
T_p	52	N	Thrust
ρ	1025	kg/m^2	Density of seawater

TABLE III
STABILITY DERIVATIVE VALUES IN (1)–(6)

$Y_{\dot{v}}$	-595.0	kg	Added mass
$Y_{\dot{r}}$	-57.91	kg	
$N_{\dot{v}}$	-57.91	kg-m^2	Added Inertia
$N_{\dot{r}}$	-381.4	kg-m^2	
Y_v	-106.0	kg/m	Force deriv.
Y_r	37.90	kg	
N_v	-494.9	kg	Munk moment
N_r	-288.1	kg-m	Torque deriv.

TABLE IV
HYDRODYNAMIC VALUES FOR RING WING IN (1)–(6)

d_R	0.381	m	Diameter
c_R	0.127	m	Chord
$C_{L\alpha}$	4.80	radians^{-1}	Coef. of lift slope
C_{Do}	0.012	none	Coef. of drag

TABLE V
HYDRODYNAMIC VALUES FOR RING-WING STRUTS IN (1)–(6)

b_S	0.127	m	Span
$\bar{c}_S$	0.043	m	Chord
$C_{SL\alpha}$	6.28	radians^{-1}	Coef. of lift slope
C_{SDo}	0.012	none	Coef. of drag

TABLE VI
HYDRODYNAMIC VALUES FOR GPS/RF ANTENNA FIN IN (1)–(6)

b_F	0.254	m	Span
$\bar{c}_F$	0.0762	m	Chord
$C_{FL\alpha}$	4.4	radians^{-1}	Coef. of lift slope
C_{FDo}	0.005	none	Coef. of drag

TABLE VII
HOMING CONTROL GAINS IN FIG. 6

K_p	0.4	none	Position gain
K_r	2.0	seconds	Rate gain
K_v	0.0	radians/meter/second	Lateral speed gain
K_I	0.02	seconds^{-1}	Integral gain
T	0.2	seconds	Sampling period

TABLE VIII
DOCKING CONTROL GAINS IN FIG. 8

K_p	1.0	none	Position gain
K_r	2.0	seconds	Rate gain
K_v	0.0	radians/meter/second	Lateral speed gain
K_{wp}	0.05	radians/meter	Wpnt. posn. gain
K_{Iwp}	0.003	radians/second/meter	Wpnt. intgrl. gain
T	0.2	seconds	Sampling period
a	1/2.5	seconds^{-1}	Filt. nat. freq.
K	$1 - e^{aT}$	none	Filt. gain

ACKNOWLEDGMENT

This work would not have been possible without the sustained effort of the entire MBARI Docking team, including J. Erickson, T. Hoover and F. Shane, as well as important contributions from H. Thomas, R. Henthorn, J. Connor (MBARI), S. Rock (Stanford University), and others. The authors would particularly like to thank T. Stanton (Naval Postgraduate School) for providing the ADCP data in Figs. 14 and 15, and also allowing them full and unrestricted access and use of the Monterey Inner Shelf Observatory, which provided the undersea power and data cable, and infrastructure required to support the dock.

REFERENCES

[1] J. Evans, P. Redmond, C. Plakas, K. Hamilton, and D. Lane, "Autonomous docking for intervention-style AUVs using sonar and video-based real-time 3D pose estimation," in *Proc. MTS/IEEE OCEANS Conf.*, San Diego, CA, Sep. 2003, pp. 2201–2210.

[2] T. Fukasawa, T. Noguchi, T. Kawasaki, and M. Baino, "Marine bird—A new experimental AUV with underwater docking and recharging system," in *Proc. MTS/IEEE OCEANS Conf.*, San Diego, CA, Sep. 2003, pp. 2195–2200.

[3] H. Singh, J. G. Bellingham, F. Hover, S. Lerner, B. A. Moran, K. Heydt, and D. Yoerger, "Docking for an autonomous ocean sampling network," *IEEE J. Ocean. Eng.*, vol. 26, no. 4, pp. 498–513, Oct. 2001.

[4] B. Allen, T. Austin, N. Forrester, R. Goldsborough, A. Kukulya, G. Packard, M. Purcell, and R. Stokey, "Autonomous docking demonstrations with enhanced REMUS technology," in *Proc. MTS/IEEE OCEANS Conf.*, Boston, MA, Sep. 2006, pp. 1–6, doi: 10.1109/OCEANS.2006.306952.

[5] R. Stokey, B. Allen, T. Austin, R. Goldsborough, N. Forrester, M. Purcell, and C. V. Alt, "Enabling technology for REMUS docking: An integral component of an autonomous ocean sampling network," *IEEE J. Ocean. Eng.*, vol. 26, no. 4, pp. 487–497, Oct. 2001.

[6] S. Cowen, S. Briest, and J. Dombrowski, "Underwater docking of an autonomous undersea vehicle using optical terminal guidance," in *Proc. MTS/IEEE OCEANS Conf.*, Halifax, NS, Canada, Oct. 1997, pp. 1143–1147.

[7] P. M. Lee, B. H. Jeon, and S. M. Kim, "Visual servoing for underwater docking of an autonomous vehicle with one camera," in *Proc. MTS/IEEE OCEANS Conf.*, San Diego, CA, Sep. 2003, pp. 2195–2200.

[8] ***[AU: Please provide city and state of the institution]***M. Gertler, "Resistance experiments on a systematic series of streamlined bodies of revolution—For application to the design of high-speed submarines," Navy Department, The David Taylor Model Basin, Rep. C-297, Apr. 1950.

[9] ***[AU: Please provide page range]***R. S. McEwen and K. Streitlien, "Modeling and control of a variable-length AUV," in *Proc. 12th Int. Symp. Unmanned Untethered Submersible Technol.*, Durham, NH, Aug. 2001.

[10] M. D. Feezor, F. Y. Sorrel, P. R. Blankenship, and J. G. Bellingham, "Autonomous underwater vehicle homing/docking via electromagnetic guidance," *IEEE J. Ocean. Eng.*, vol. 26, no. 4, pp. 515–521, Oct. 2001.

[11] ***[AU: Please provide page range]***J. G. Bellingham, R. S. McEwen, and B. W. Hobson, "The development of a docking station for a regional cabled observatory," in *Proc. 4th Int. Workshop Scientific Use of Submarine Cables*, Dublin, Ireland, Feb. 2006.

[12] ***[AU: Please provide volume and issue]***R. Coulson, J. Lambiotte, and E. An, "A modular docking system for 12.75-inch class AUVs," *Sea Technol.*, pp. 49–54, Apr. 2005.

[13] ***[AU: Please provide city and state of the institution]***M. Gertler and G. Hagen, "Standard equations of motion for submarine simulation," David W. Taylor Naval Ship Research and Development Center, Rep. 2510, 1967.

[14] T. I. Fossen, *Guidance and Control of Ocean Vehicles*. New York: Wiley, 1994.

[15] M. Guelman, "A qualitative study of proportional navigation," *IEEE Trans. Aerosp. Electron. Syst.*, vol. AES-7, no. 4, pp. 637–643, Jul. 1971.

[16] T. Stanton, Monterey Inner Shelf Observatory Web Page Moss Landing, CA [Online]. Available: http://www.oc.nps.navy.mil/~stanton/miso

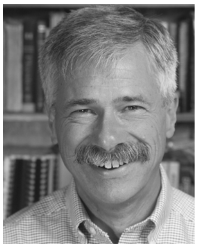

Robert S. McEwen (M'99) was born in Cleveland, OH, in 1955. He received the B.S. degree in electrical engineering from Purdue University, West Lafayette, IN, in 1978, the M.S. degree in electrical engineering from the University of Illinois, Chicago, in 1982, and the M.S. degree in mechanical engineering from Stanford University, Stanford, CA, in 1988. His specialization was dnamics and control.

He worked at Lockheed Corporation from 1982 to 1988 on spacecraft attitude control and navigation. From 1988 to 1997, he worked at Integrated Systems Incorporated on a variety of control-system related projects, from automotive power steering to spacecraft control. He was the Principal Engineer for the control system of the Miniature Sensor Technology Integration (MSTI) spacecraft, which operated successfully in orbit for over a year, exceeding its design life. Since 1998, he has worked primarily on autonomous underwater vehicle (AUV) guidance, navigation, and control systems for the Monterey Bay Aquarium Research Institute, Moss Landing, CA.

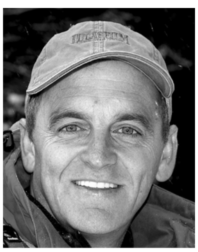

Brett W. Hobson (M'98) received the B.S. degree in mechanical engineering from California State University, San Francisco, in 1989.

Currently, he is working with the Platforms Group within the R&D Department, Monterey Bay Aquarium Research Institute (MBARI), Moss Landing, CA. Before joining MBARI, he helped start Nekton Research, a Navy R&D contractor specializing in small underwater vehicles. He started designing, building, and operating undersea systems at Deep Ocean Engineering and Deep Sea Discoveries.

Mr. Hobson is a member of the Marine Technology Society and American Geophysical Union.

Lance R. McBride (M'96) received the B.S. degree in electrical engineering from Walla Walla College, College Place, WA, in 1996.

He has worked in the fields of network engineering, particle acceleration, high-speed video electronics, and oceanographic equipment. He is currently consulting as an Electrical Engineer, and was formerly an Electrical Engineer with the Research and Development Department, Monterey Bay Aquarium Research Institute (MBARI), Moss Landing, CA. His professional interests include low-power electronics, imaging systems, human interface technology, and circuit card design. He has authored and coauthored numerous publications for the IEEE Oceanic Engineering Society and other publications.

Mr. McBride has been a member of the Association for Computing Machinery (ACM) and was a licensed Microsoft Certified Systems Engineer (MCSE). He was the president of his IEEE student body during his senior year at Walla Walla College, and was awarded third place for his IEEE student entry at the Columbia Basin Technical Conference and Trade Show in 1996. He has been a Registered Professional Engineer in the State of California since 2006.

James G. Bellingham (M'XX)***[AU: Please provide membership year. The information was not found in the IEEE database. Please provide educational background]***

Currently, he is the Chief Technologist at the Monterey Bay Aquarium Research Institute (MBARI), Moss Landing, CA. His personal research activity revolves around the development and use of autonomous underwater vehicles (AUVs). In the process of developing these vehicles, he spent considerable time at sea, leading over 20 AUV expeditions. He leads the Autonomous Ocean Sampling Network (AOSN) program at MBARI, which uses fleets of autonomous vehicles to adapt to and observe rapidly changing oceanographic processes.

Docking Control System for a 54-cm-Diameter AUV

Robert S. McEwen, *Member, IEEE*, Brett W. Hobson, *Member, IEEE*, Lance McBride, *Member, IEEE*, and James G. Bellingham, *Member, IEEE*

***Abstract*—The Monterey Bay Aquarium Research Institute (MBARI, Moss Landing, CA) has developed a 54-cm-diameter (21-in) docking AUV and companion docking station. This program resulted in four consecutive successful autonomous homing and docking events in the open ocean, which included downloading data, uploading a new mission plan, recharging the battery, and complete power cycling of the AUV. We describe the design, simulation, and at-sea test of the homing and docking control system.**

***Index Terms*—Autonomous underwater vehicle, docking, control system, mobile robot, sonar homing.**

I. Introduction

AUTONOMOUS underwater vehicles (AUVs) are playing a growing role in the ocean sciences. At Monterey Bay Aquarium Research Institute (MBARI, Moss Landing, CA), a 6-km-depth-rated mapping AUV is routinely generating bathymetry maps with unprecedented precision, resolution, and speed, and a second AUV routinely performs physical, chemical, and biological measurements in Monterey Bay. Both of these AUVs are characteristic of a class of vehicles carrying sophisticated, but power-intensive instrumentation. The high-power draw of the instrumentation limits today's AUVs to endurances of roughly one day. This means that for all but near-shore operations, the vehicles must be attended by a ship. As a consequence, the fundamental utility of the AUV is limited by ship support requirements. In some cases, the issue is cost. In other cases, the need for ship support makes activities impossible, for example, in high sea states, or when events cannot be predicted in advance for scheduling ship time.

Our docking station is designed to link to the power and communication infrastructure of a seafloor observatory, enabling the AUV to operate independently of a surface vessel for extended periods. In effect, the docking station allows the vehicle to connect to a mooring or a cabled instrumentation node. While docked, the AUV can recharge its batteries, download data, upload new instructions, and safely park until the next mission.

Manuscript received January 24, 2008; accepted August 21, 2008. This work was supported in part by the National Science Foundation under Grant NSF-OPP 9910290. Any opinions, findings, and conclusions or recommendations expressed in this material are those of the authors and do not necessarily reflect those of the National Science Foundation. This work was also supported by the David and Lucile Packard Foundation.

Associate Editor: L. Whitcomb.

R. S. McEwen, B. W. Hobson, J. G. Bellingham are with the Monterey Bay Aquarium Research Institute (MBARI), Moss Landing, CA 95039-9644 USA (e-mail: rob@mbari.org; hobson@mbari.org; jgb@mbari.org).

L. McBride was with the Monterey Bay Aquarium Research Institute (MBARI), Moss Landing, CA 95039-9644 USA (e-mail: lance.mcbride@ieee.org).

Color versions of one or more of the figures in this paper are available online at http://ieeexplore.ieee.org.

Digital Object Identifier 10.1109/JOE.2008.2005348

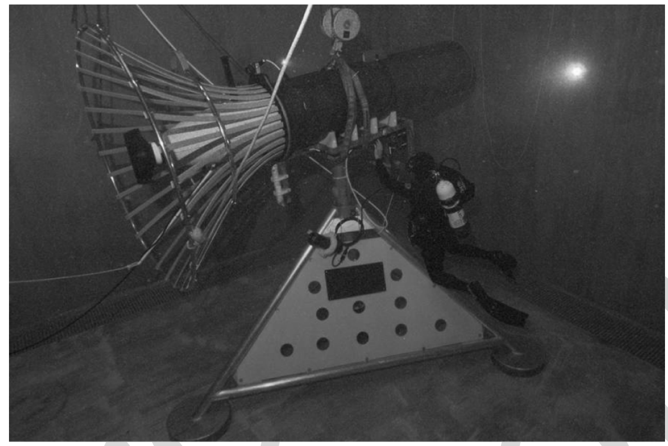

Fig. 1. AUV in the dock in a seawater test tank.

Once its batteries are recharged, the AUV can be deployed nearly instantaneously. Instead of being limited to studying static or repetitive subjects, the AUV can be dispatched on short notice to record episodic events such as canyon turbidity flows or plankton blooms, greatly increasing its scientific utility.

The move toward seafloor observatories is international in scope and creates the possibility that power and communication infrastructure will be available on the seafloor in a variety of interesting regions. At MBARI, the focus has been the development of the Monterey Accelerated Research System (MARS)-cabled observatory and the Monterey Ocean Observing System (MOOS) mooring-based observatory. MARS is a testbed for subsequent cabled observatories, and it provides an early opportunity to develop and demonstrate the AUV docking capability in a logistically benign environment. The compatibility of MARS and the docking system should ensure that the system is well suited to being deployed on future regional-scale cabled observatories (RCOs). The MOOS mooring system is also capable of supporting docking, and while MOOS is unable to supply as much power to a docking station as a shore-cabled observatory, it has the advantage of being much more easily relocated and deployed in regions of interest.

In the tests described below, the AUV was able to successfully dock and undock repeatedly in the open ocean, without assistance from the surface. Shore operators downloaded mission data and uploaded the next mission through an underwater Ethernet link, charged the battery, and completely powered the vehicle down and back up. Fig. 1 shows the dock and the vehicle in a test tank.

Fig. 2 shows the vehicle entering the dock in the Monterey Bay where the AUV was tested in a near-shore, disturbance-intensive environment. The dock worked well despite the fact that it was designed for a permanent deployment in a deeper,

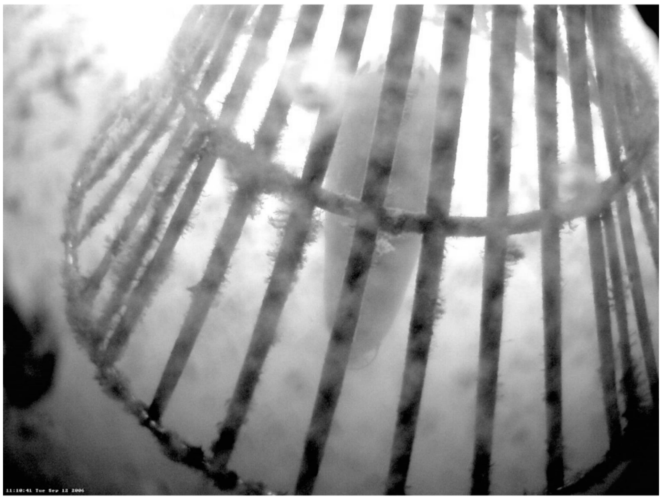

Fig. 2. AUV entering the dock in Monterey Bay.

more benign environment at the MARS-cabled observatory at 900-m depth in Monterey Bay. This deeper MARS site is free from surface wave motion and the intensive biofouling evident in Fig. 2.

II. Docking System Options

In past years, various research groups have developed different and innovative dock designs. Some of these require a hovering vehicle, such the intervention-style grappling system described in [1]. Another hovering vehicle has a tail hook and wire arrangement, where the vertical thrusters lower the vehicle into a cradle [2]. The designs of docks for flying vehicles, which rely on sustained forward motion for control, generally are either a pole or funnel type. In the pole design [3], the vehicle carries a latching mechanism that grabs on to a vertically moored pole or cable. In the funnel or cone design, the vehicle enters a circular funnel and is channeled into a tube where it is captured. There have been several designs of this type for smaller vehicles: the Remus/LEO15 system [4], [5], the Flying Plug [6], and the KRISO-KORDI [7]. To the best of our knowledge, there has never been a cone dock for a 54-cm-vehicle (21 in) that worked in the ocean.

We considered three classes of dock for MBARI's torpedo-like flying vehicle: the pole, the weathervaning cone, and the fixed cone. The pole is omnidirectional and eases the constraint on depth control, but requires the vehicle to carry an external, complex, motorized latching device. Establishing the power and data connection is difficult because the docked vehicle is not rigidly attached to the pole. A weathervaning cone is also omnidirectional, but securely captures the vehicle, making power and data connections easier. However, the dock must communicate its heading to the vehicle before docking, requiring a bidirectional communication system. This design must also transfer power and data across a moving interface, most likely using a slip ring. After considering these options, we chose the fixed cone primarily for its simplicity. Section IV describes the design in detail.

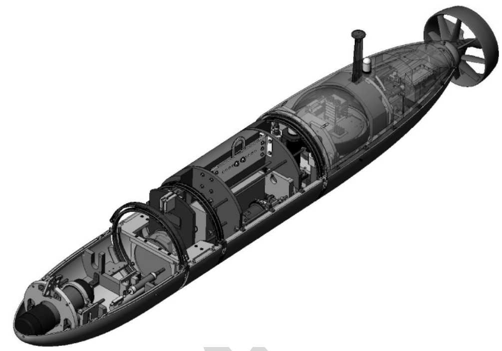

Fig. 3. Solid model of the docking AUV showing ultrashort base line (USBL) homing system as a cylinder in the bow.

III. The Autonomous Underwater Vehicle

The docking AUV is a Dorado/Bluefin 54-cm-diameter type (21 in), which has a Gertler body shape, series 58 model 4154, with a cylindrical midsection inserted at the point of maximum diameter, and a ring-wing tail [8], [9]. The vehicle is 358 cm long, and weighs 640 kg including entrained water. The vehicle has the capacity to carry three pressure-tolerant batteries, although during the short duration docking sea trials, it typically carried only one. Each battery provides 2 kWh of energy, giving a maximum range of approximately 70 km at 1.5 m/s with all three batteries present. The vehicle must maintain a minimum speed of approximately 0.8 m/s for controllability and to counteract the static buoyancy.

The ring-wing control and propulsion unit is shown in Fig. 3. A fractional horsepower direct current (dc) brushless motor with a 10 : 1 reduction gear box generates 52 N of thrust at 300 r/min. The ring wing is attached to a double-gimbal by eight equally spaced struts, which are small foils with a twist or preswirl. See Tables IV and V for numerical values, and [9] for a photograph and a mathematical model. Both the ring and the struts are based on a NACA ***[AU: Please define NACA]*** 0015 foil profile.

Gimbaling the ring and thruster together provide the control forces. At 3 kn, the lift from the ring is larger by about a factor of five than the lateral component of vectored thrust.

The control system consists of outer and inner proportional–integral–derivative (PID) loops for both heading and depth. The nominal horizontal-plane cross-track control loop is similar to the docking control presented in Fig. 8. A full explanation of the control system in both vertical and horizontal planes is in [9].

The vehicle navigation system is essentially Doppler velocity log (DVL)-aided dead reckoning, with periodic global positioning system (GPS) updates, which require surfacing. The expected accuracy is 4% of distance traveled (DT), circular error probability (CEP) with the navigation and control sampling rate of 5 Hz.

The AUV homes to the dock using an ultrashort base line (USBL) sonar transceiver mounted in the vehicle nose, as shown in Fig. 3. MBARI selected a Sonardyne-Scout-inverted USBL homing system, although other types of homing systems have been proven, such as an electromagnetic system [10] and optical systems [6] and [7]. The USBL has the advantage of much greater range and is also reliable, mature, and commercially available. The only drawback is that the Sonardyne Scout USBL selected is relatively large and takes up valuable space in the nose of the AUV. The USBL provides a bearing to its beacon in both the horizontal and vertical planes with a specified accuracy of 0.28° root mean square (RMS). The maximum sampling frequency of the USBL is 1 Hz due mostly to the beacon turnaround time and subsequent beacon lockout, which are 300 and 600 ms, respectively. Sonardyne reportedly is considering a faster beacon firmware design, which assumes a single, nearby vehicle. This sampling rate may go as high as 3 Hz.

The USBL is also useful as a general navigation instrument, because it provides position fixes much like GPS, but without surfacing or stopping. MBARI has already placed and surveyed over 100 USBL beacons in Monterey Bay, most of which are available for navigation.

IV. The Dock

The MBARI design approach keeps the dock as simple as possible and puts the complexity on the vehicle, because it is easier to retrieve the vehicle for maintenance. The dock is a benthic, fixed-heading cone with minimal moving parts and electronics. The cone design does not require the vehicle to carry an external latching mechanism, and also provides secure parking and a rigid data/power connection. The drawback is that the vehicle must fly with a near-bottom precision approach along a fixed flight path, possibly in a cross current, and must therefore contain the necessary electronics and algorithms.

The dock's entry is conically shaped, built of fiberglass staves held in place by two tubular stainless steel rings with an entrance diameter of 2 m. This entrance diameter was selected based on the following:

1) observations that the vehicle was passing well within two meters of the transponder during initial homing tests [11];
2) the predicted position deviation of the vehicle described in Section IX using the data from Section XI;
3) personal communications from local divers familiar with bottom currents in that area.

The dock body, consisting of the cone and the tube, is mounted on a 3-m-tall aluminum tripod (Fig. 1). The tube is made of fiberglass, and is of diameter 57 cm, 3 cm wider than the vehicle's diameter. An external pressure housing contains the electronics necessary to support power and data transfer between the vehicle and the cable. A USBL homing beacon is mounted below the front of the tube and is visible in Fig. 1. The small black cylinder at the top of the pyramidal base is a video camera, which turned out to be extremely useful for understanding dock/vehicle interaction dynamics and verifying missed distance measurements made by the USBL.

Although the dock body is fixed in heading, it gimbals in pitch and roll, due to a self-leveling pendulum designed for deployment on a sloped bottom at MARS. During ocean testing in relatively shallow water, described in Section X, the forces exerted by the short-period wave motion caused the dock to continually pitch up and down with an amplitude of approximately 10°–15°. This motion proved to be helpful in preventing the AUV from binding during entry. A next generation dock design will likely take more deliberate advantage of this pitching motion to prevent binding, as well as employing other aids such as mechanical rollers.

The vehicle is mechanically latched by a motorized peg that inserts into the AUV. We expect that a next generation design will reverse the peg and socket, placing the moving peg in the vehicle, in keeping with our design philosophy of an uncomplicated dock. Even with the peg located in the dock, the entire docking system has only a single drive motor and associated moving part.

The position of the vehicle in the dock is sensed by a pair of inductors: one mounted in the top of the vehicle, and the other fixed at a corresponding location in the docking tube. These have a range of several centimeters, and provide the trigger to raise the latching peg. These sensors were part of a docking module assembly that Florida Atlantic University (FAU, Boca Raton) developed under a grant from the U.S. Office of Naval Research (Arlington, VA) [12], and that we obtained from them. It is described further below.

V. Power and Data Transfer

Power transfer was accomplished by a transformer coil embedded in the tip of the latching peg and a corresponding coil in the socket. The system then transfers power inductively through the seawater without a metal-to-metal connection. The inductive power transfer subsystem was developed at FAU and was adapted for use on the Monterey Inner Shelf Observatory (MISO) cable where the sea trials were conducted. The adaptions included minor software modifications, and two Vicor dc : dc converters to convert from +300 V_{dc}, coming in from the cable, to +48 V_{dc}, required by the FAU module, and to +12 V_{dc} for the Ethernet wireless access points.

While deployed at sea, the power transfer was tested over a period of 10 min by charging the vehicle's battery. Measurements on shore showed 416 W delivered from shore, and measurements on the vehicle showed a total of 61.5 kJ were transferred into the battery. The efficiency of the inductive units was 77% with an overall power system efficiency of 48%. To improve the overall power system efficiency, the dock-side dc–dc converter would need to be redesigned to run directly off of the 300 V_{dc} shore voltage.

The system is built so that the vehicle can be completely shut off while in the dock. The vehicle is restarted by applying power first to the vehicle's FAU inductive unit, which then provides power to the bus. After the vehicle's computer has booted, communications can then be reestablished between the computer and shore-side server by the wireless communications link. This power-saving feature was tested and verified at sea.

The AUV forms a wireless network link with the dock using modified off-the-shelf Ethernet antennas. One is embedded in the top of the vehicle, with its mate correspondingly located in the top of the docking tube. The static vehicle buoyancy holds the antennas nearly in contact, with the peg aligning the vehicle fore and aft. The link was developed to provide a 10 Mb/s data path across a 6.35-cm seawater gap. It is based on IEEE 802.11 and is fully compatible with the Ethernet network used throughout the vehicle and dock. The full specifications for the

TABLE I
DEPLOYED UNDERWATER WIRELESS SYSTEM PERFORMANCE SPECIFICATIONS

Protocol	802.11g
Transmission Frequency	2.4 GHz
RF Power	1 W
Antenna	0.22 λ_{air} whip
RF Link Margin	21.7 dB
Demonstrated seawater transmission distance	6.35 cm
Deployed seawater transmission distance	3.81 cm
ICMP transmission success rate	98.85%
Average ICMP time	4 ms
Bandwidth	9.5 Mb/s

link are shown in Table I. This system worked reliably during the sea trials.

VI. HOMING AND DOCKING SEQUENCE

The general homing and docking sequence consists of the following steps.

1) Locate and home to the dock. The vehicle uses its onboard navigation to transit within USBL range of the beacon, about 2 km. The USBL is directional with a ±85° field of view. The vehicle then homes to the dock using pure pursuit guidance, where the heading control system continuously points the vehicle at the beacon. This guidance strategy does not compensate for ocean current and thus the vehicle can be blown downwind while approaching. Pursuit guidance has the advantage of keeping the USBL pointed at the beacon for maximum signal strength.
2) Compute a position fix. When the USBL attains good signal strength, the vehicle uses its compass heading and the USBL bearing and range to compute a position fix. Based on previous testing, this occurs between 1000 and 200 m away from the dock. Because the homing control does not use compass heading or propagated position, a jump in the propagated position caused by the fix does not affect the vehicle control.
3) Fly to the start of the final approach path. The approach path is along the cone centerline, and begins about 300 m out. The approach may require the vehicle to turn away from the dock and temporarily lose USBL contact.
4) Execute final approach. The vehicle approaches along the cone centerline using a cross-track controller instead of pure pursuit. This means that the vehicle will track the approach path to the cone, and acquire a drift correction angle (crab angle) if the ocean current has a lateral component. This type of control uses both range and bearing from the USBL at 1 Hz, and uses the DVL and compass to dead-reckon between USBL updates. The vehicle slows to 1.0 m/s about 200 m from the dock. This allows time for the control loop to zero the cross-track error, and also prevents the vehicle from hitting the dock with too much force.
5) Latch. The vehicle uses the inductive position sensor and Ethernet contact to determine if it has fully entered. The algorithm then raises the peg and latches the vehicle.

The vehicle's automatic peg-raising code was not fully debugged at the time of the sea trials and worked sporadically in the preceding tank tests. During the sea trials, shore operators manually raised the pin by watching the vehicle enter the dock on camera. The Ethernet path from the main vehicle computer to the peg PIC passed through four wireless access points (WAPS), and we believe the source of the problems lay in the four routing tables.

Fig. 4 shows the various possibilities during the homing and docking sequence in state-diagram form. Step 1 of the enumerated list corresponds to the "homing" state in the figure, step 3 to "transit to outer marker," and step 4 to "docking." Items shown with an asterisk were planned but not implemented at the time of these tests.

The ability of the vehicle to sense a deceleration without network presence, that is, to sense that it is stuck either partially in the dock, or somewhere else, was not implemented for the sea trials, but is important and planned for later development. To account for this during the sea trials, we appended a time delay followed by a full reverse thrust behavior to the end of each mission. If the vehicle became stuck, it would run through the rest of the mission in place, but would end by reversing thrust, thus possibly freeing itself. In case the vehicle missed the dock, shore operators could simply terminate the mission over the radio modem after the vehicle surfaced but before the reverse thrust started.

The homing and docking states and associated control loops were tested separately. Homing was tested in fall 2005 in central Monterey Bay off Moss Landing. Docking was tested during summer and fall 2006 offshore Monterey Bay where the dock was attached to an underwater cable, as described in Section X.

The position fix update in step 2 was not implemented in time for the sea trials. However, it is straightforward and would eliminate surfacing the AUV for a GPS fix close to the dock, which would be impractical in the relatively deep water at the MARS location.

VII. UNDOCKING

The vehicle was designed to undock by lowering the peg and reversing the thruster. The vehicle is unstable in reverse, and therefore, thrusts with a fixed elevator angle and short duration. After the thruster shuts off, the vehicle floats up to a specified altitude that is above and clear of the dock. The vehicle then begins a normal mission with ahead thrust, which consists of a U-turn and a transit back to the outer waypoint.

During the sea trials, the shore operators manually lowered the peg and initiated the undocking mission while watching on the camera, because the vehicle's onboard peg control code was not yet reliable.

A planned, but not implemented feature, was an undocking behavior that would pulse the thruster forward and backward to break loose if the vehicle had difficulty backing out. Should the vehicle become permanently stuck, the final dock design would contain an acoustic release at the top of the base, and the rest of the dock would be positively buoyant. A support ship could then trigger the release and recover both the vehicle and the dock.

VIII. HOMING CONTROL LOOP

This section explains the homing control loop that operates in step 1 (Section VI). Section IX explains the docking control loop of step 4.

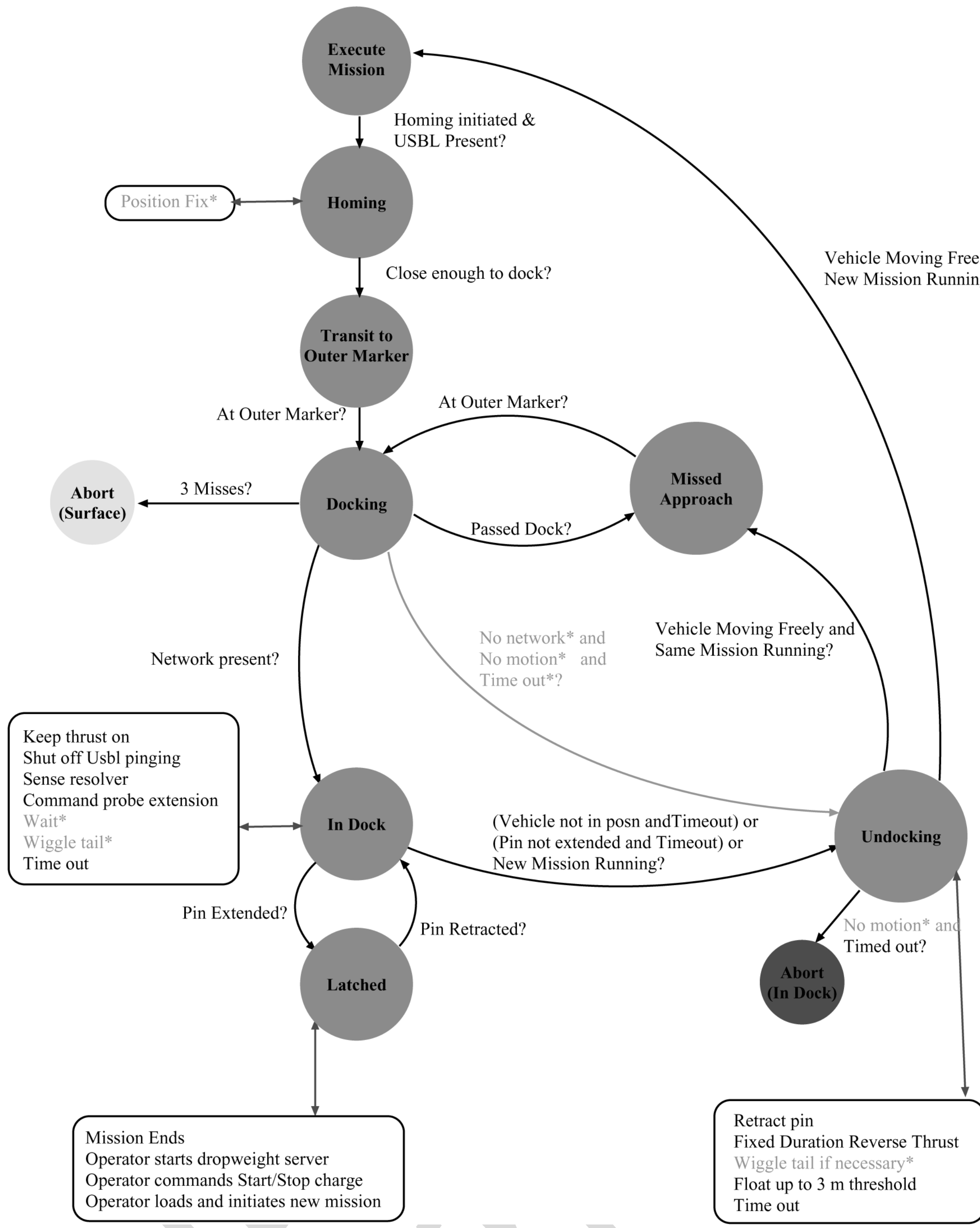

Fig. 4. State diagram of the mission, homing, and docking sequence. An asterisk indicates a planned item, not yet implemented during sea trials.

Fig. 5 shows angle and reference frame definitions used in the following homing analysis. Angles are defined to be positive clockwise.

The design and analysis of the homing and docking control loops are fundamentally based on the dynamics of the vehicle, described by coupled nonlinear equations of motion (EOM) such as those in [13]. The vehicle travels in straight and level flight when approaching the dock, with small angular and translational deviations, in which case the horizontal-plane and vertical-plane dynamics decouple. Equation (1), shown at the top of the next page, is the horizontal-plane, or sway-yaw dynamics linearized about straight and level flight. It is fourth order and consists of $\Delta\psi$, heading deviation; y, cross-track displacement; v, lateral velocity component in the body frame; and finally, r, which is heading rate. See [14, p. 117] and [9] for derivations. Tables II–VI in the Appendix define the symbols and numerical values of the constants.

The depth control did not require any special modifications for docking, and so discussion of the vertical-plane dynamics and control [9] are not repeated here.

The origin of body-fixed coordinate system assumed by (1), and the values in Tables II and III, is amidships, that is, along

$$
\begin{bmatrix} m - Y_{\dot v} & mx_G - Y_{\dot r} & 0 & 0 \\ mx_G - N_{\dot v} & I_{zz} - N_{\dot r} & 0 & 0 \\ 0 & 0 & 1 & 0 \\ 0 & 0 & 0 & 1 \end{bmatrix} \begin{bmatrix} \dot v \\ \dot r \\ \dot y \\ \Delta\dot\psi \end{bmatrix}
= \begin{bmatrix} (Y_v - Y_{\mathrm{RF}} - Y_A)U & (Y_r - m - x_R Y_{\mathrm{RF}} - x_A Y_A)U & 0 & 0 \\ (N_v - x_R Y_{\mathrm{RF}} - x_A Y_A)U & (N_r - mx_G - x_R^2 Y_{\mathrm{RF}} - x_A^2 Y_A)U & 0 & 0 \\ 1 & 0 & 0 & U \\ 0 & 1 & 0 & 0 \end{bmatrix} \begin{bmatrix} v \\ r \\ y \\ \Delta\psi \end{bmatrix}
+ \begin{bmatrix} Y_R U^2 + T_P \\ (Y_R U^2 + T_P)x_R \\ 0 \\ 0 \end{bmatrix} \delta_R - \begin{bmatrix} (Y_v - Y_{\mathrm{RF}} - Y_A)U \\ (N_v - x_R Y_{\mathrm{RF}} - x_A Y_A)U \\ 1 \\ 0 \end{bmatrix} v_c \quad (1)
$$

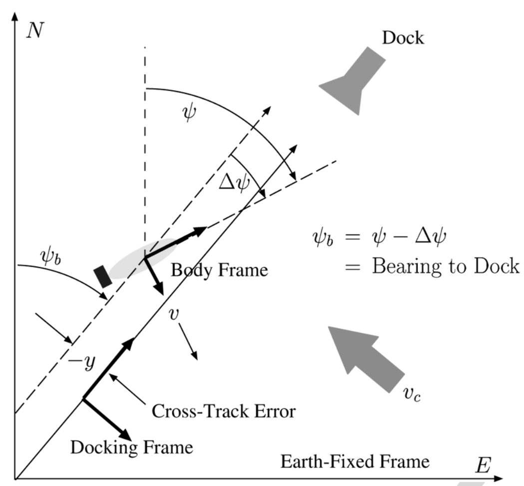

Fig. 5. Angle and reference frame definitions: y is the lateral displacement of the vehicle from the dock centerline, $\Delta\psi$ is the dock-relative heading, and v_c is cross current.

the centerline at half the overall length. It is *not* at the center of mass or the center of buoyancy.

Although the control surface is a double-gimbaled ring wing, small motion about the vertical axle is termed "rudder motion," and "elevator motion" is about the horizontal axle. In (1), Y_{RF} is the sway force coefficient due to the ring fixed in the neutral position

$$Y_{\mathrm{RF}} = \frac{1}{2}\rho A(C_{L\alpha} + C_{Do}) + \frac{1}{2}\rho A_S(C_{SL\alpha} + C_{SDo}). \quad (2)$$

Here the subscript RF denotes rudder fixed.

A is the area of the ring, defined as chord × diameter, that is

$$A = \bar c_R d_R. \quad (3)$$

A_S is the equivalent strut area, defined to be

$$A_S = 2(1 + \sqrt{2})\bar c_S b_S. \quad (4)$$

$C_{L\alpha}$ is the slope of the coefficient of lift of the ring, and C_{Do} is the coefficient of drag. Similar symbols with subscripts S and F refer to the struts and RF/GPS fin, respectively. It is common to subsume the rudder-fixed portion of the force Y_{RF} into the stability derivatives. In this presentation, Y_{RF} is added explicitly in (1), and so the stability derivative values in Table III are for the fuselage only.

Y_A is the sway force due to the RF/GPS antenna fin

$$Y_A = \frac{1}{2}\rho A_F(C_{FL\alpha} + C_{FDo}) \quad (5)$$

where A_F is the area. Fig. 1 shows the fin.

Y_R is the sway force coefficient due to a deflected rudder

$$Y_R = \frac{1}{2}\rho A C_{L\alpha}. \quad (6)$$

v_c is cross current, modeled as a disturbance input, and it is shown in Fig. 5.

The homing control loop implements pure pursuit guidance, which requires that the vehicle's nose continuously point at the beacon during the approach. Pure pursuit is a special case of the well-known proportional navigation technique used for missile guidance [15]. Pure pursuit is proportional navigation with a gain of unity. Larger gains will cause the pursuing vehicle to lead the target and intercept faster, but the algorithm is more complicated. Proportional navigation is unnecessary in our case because the time-to-intercept is unimportant, and also because the vehicle does not come directly into the dock, but must first transit over to a fixed approach path after it gets to ***[AU: "gets to" what? Is something missing here?]***with several hundred meters. The dock has a fixed heading and the vehicle must line up with it, much like an airplane approaching a runway.

When the homing loop is first initiated, it uses cross-track waypoint control to fly toward a preprogrammed dock location until the USBL receives a response from the beacon. From that point on, the algorithm latches the beacon location, and flies towards that point until the USBL updates with a new location. Updates occur every one to three seconds depending on range.

Fig. 6 shows the homing control loop. It is multirate PID with the option for feedback on the lateral speed state v. The lateral speed feedback term was not used in the final design. The cross-track state y and compass heading state ψ are unnecessary for homing and are, therefore, uncontrolled and ignored.

The reference input $\Delta\psi_R$ represents the angular motion of the dock relative to the vehicle. If the AUV is being carried laterally by current, the body-referenced heading to the dock changes. Thus, this control loop needs to be able to track at low frequencies. An integrator was included in the controller

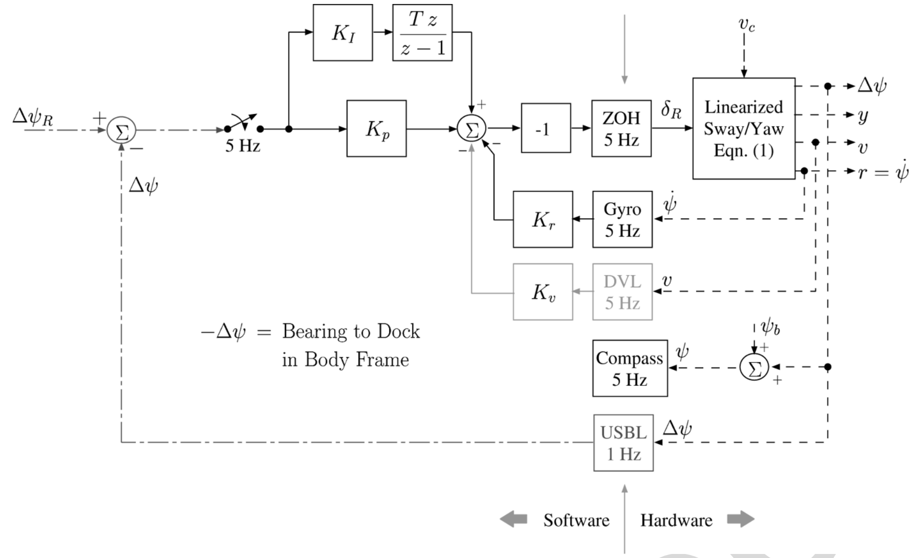

Fig. 6. Pure-pursuit homing control loop. The outer USBL loop is shown with short and long dashes because it has a sampling rate between 1 and 3 Hz, depending on the distance of the vehicle from the beacon. The rest of the system is at 5 Hz. The dashed lines indicate natural connections. The K_v rate gain was found in practice to be unnecessary and set to zero. Tables II–VI furnish the parameter values.

to give a total of two free integrators, counting the one in the plant where $\dot{\Delta\psi} = r$, as shown by (1). This closed-loop system will track constant angular motion (a ramp) with no steady-state error. Additionally, the steady-state step response to a lateral current has zero error.

A constant lateral current will cause the homing loop continuously to turn the vehicle so that as seen from above, the vehicle spirals in toward the dock. In an extreme case, the vehicle will end up approaching from down wind. Pure pursuit has the advantage of keeping the beacon centered in the USBL field of view for maximum signal strength while the vehicle gets close.

Fig. 7 shows the heading response to a $v_c = 25$ cm/s lateral current step, determined by simulation using (1). Assuming that the vehicle is at least 200 m from the dock, this heading error is insignificant because the control loop has ample time to recover. $v_c = 25$ cm/s was the maximum constant cross current expected at the test site in nonstorm conditions, and is discussed further in Section XI.

In addition to displacing the vehicle, a lateral current step exerts a yaw torque due to the lever arm between the center of pressure and the center of mass. Equation (1) models this, as shown by the N_v term in the disturbance (v_c) input matrix.

The dotted curve shows the response assuming the outer USBL loop has a sampling period of 3 s, which it does at the outer limit of its range. The inner gyro feedback loop still runs at 5 Hz. As the vehicle approaches, the USBL sampling period drops to 1 s. Fig. 7 shows that the slow outer loop does not significantly degrade the performance.

Between USBL sample periods, the 5-Hz heading loop maintains the last bearing determined by the USBL and the compass.

The control gains were empirically chosen and resulted in a dominant pole pair with a damping of 0.77 and a time constant of 17 s. This means that the vehicle will travel about 75 m before transients induced from step disturbances die out. Because we expect this loop to be in operation from 1 to 2 km out, these time constants are acceptable. Gain values are in Table VII.

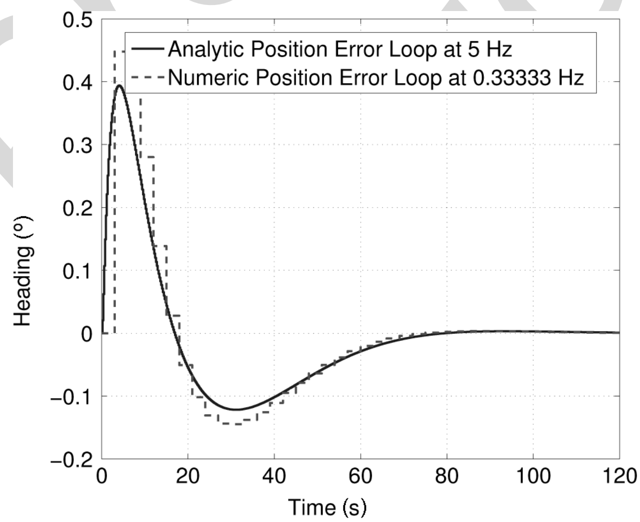

Fig. 7. Simulated closed-loop heading response to a 25-cm/s lateral step current using the control in Fig. 6.

The eigenvalues were determined by substituting analytically determined stability-derivative values into (1) and combining the result with the control loop shown in Fig. 6. Numerical values are shown in Tables II–VI.

IX. Docking Control Loop

Fig. 8 shows the docking control loop. It differs from the homing control loop because now the cross-track error state is computed from the USBL and fed back. The vehicle will now fly down a fixed approach path and will not be blown downwind by ocean currents. The integrator, which has now been moved to cross-track error, will crab the vehicle so as to keep the cross-track error at zero, should there be a cross current.

In Fig. 8, there is a smoothing filter after the waypoint control, which has a time constant of 2.5 s. This filter was neglected in

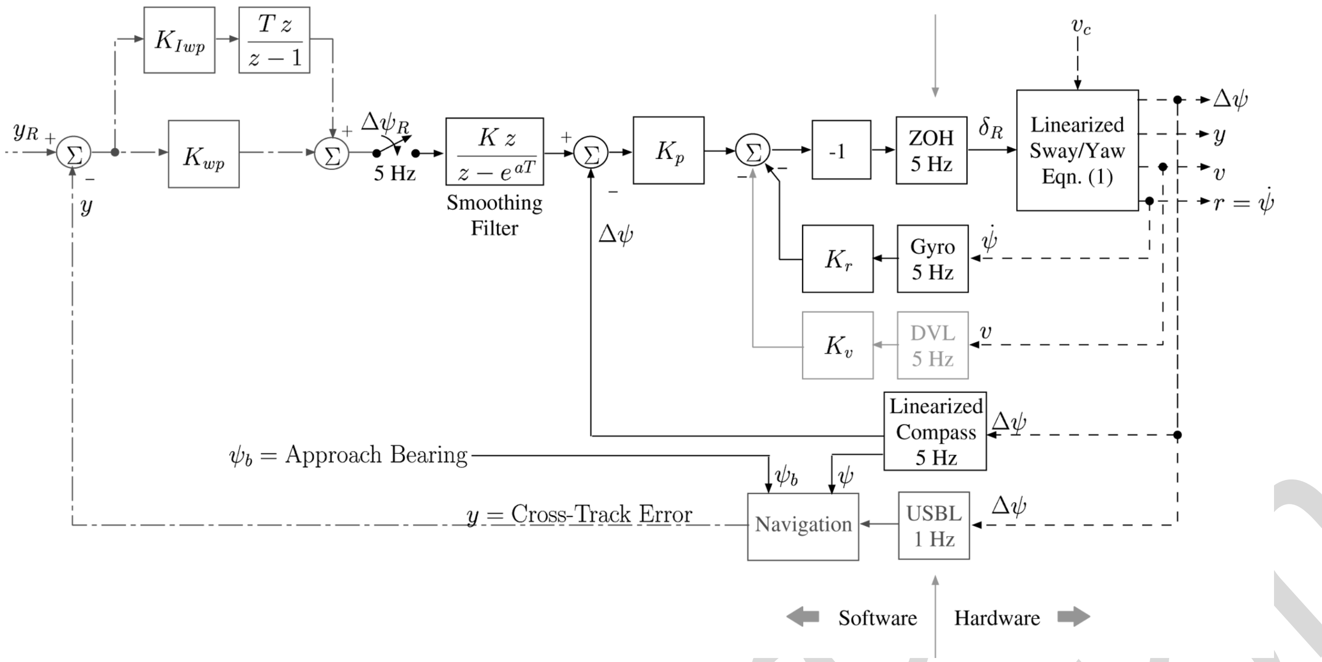

Fig. 8. Cross-track docking control loop. This system does not switch on until 200 m from the beacon. Consequently, the outer USBL loop, shown with long and short dashes, runs at about 1 Hz, as opposed to the pure pursuit system in Fig. 6, where the vehicle may be as far as 2 km away when it acquires the beacon.

the analysis below because it is much faster than the slowest roots of the closed-loop characteristic equation.

Because the vehicle position is now computed from the USBL, the navigation is free from the accruing odometry error inherent in dead reckoning. The measurement error of the USBL is proportional to the range, and thus decreases as the vehicle closes on the dock. This is fundamentally what makes the docking system work and is the reason for having a homing system.

The heading of the dock ψ_b was measured after deployment and is a known constant. It is used inside the USBL feedback loop to convert heading deviation to cross-track error.

As in the case of the homing controller, this control has a fall back in case the USBL drops out. It latches the last dock position measured by the USBL and continues by DVL-aided dead reckoning.

Control gains were again empirically determined, with K_v kept at zero. Values are shown in Table VIII. The cross-track error step response is dominated by a closed-loop pole pair with damping 0.29 and a time constant of 55 s. Fig. 9 shows simulated cross-track error response to a-25 cm/s current step.

Although the transients damp slowly, the error is well below the 1-m dock aperture radius after 100 s, while the vehicle has 100 m yet to travel before encountering the dock. This assumes that the docking control is initiated 200 m from the dock on the approach path, and the vehicle has also slowed to 1.0 m/s. The thrust is also reduced to 22 N. These two values were used in (1) along with the gains in Table VIII to produce Figs. 9 and 10.

In addition to crabbing into a constant tidal cross current, the control loop must perform in the presence of 8–12-s wave motion. The green curves in Fig. 10 show the steady-state sinusoidal response of cross-track error to lateral current. The frequency region bounded by the vertical magenta lines rep-

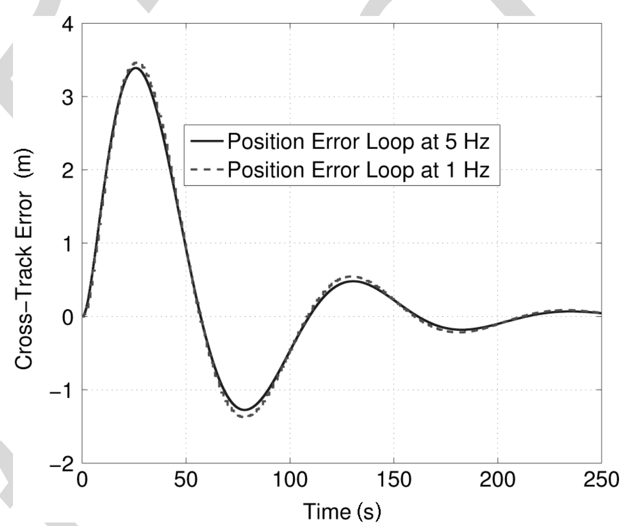

Fig. 9. Simulated closed-loop cross-track error response to a 25-cm/s lateral step current using the control in Fig. 8.

resents the wave energy. ***[AU: In many places in the paper you mention color. Please rewrite so that color is not mentioned. The figures will be published in b/w in print and in color online.]***The black curve is the open-loop transfer function, which is coincident with the closed-loop transfer function in the region of the wave energy, showing that the control loop has rolled off there and has no effect. At the low end of the wave spectrum, the closed-loop gain is a factor of 2.5, and it decreases to less than one at the high end. Typically, the wave period is close to 10 s, where the loop gain is near unity, implying that a 30-cm/s wave motion will deviate the vehicle less than 30 cm from the flight path. Close examination of ADCP ***[AU:***

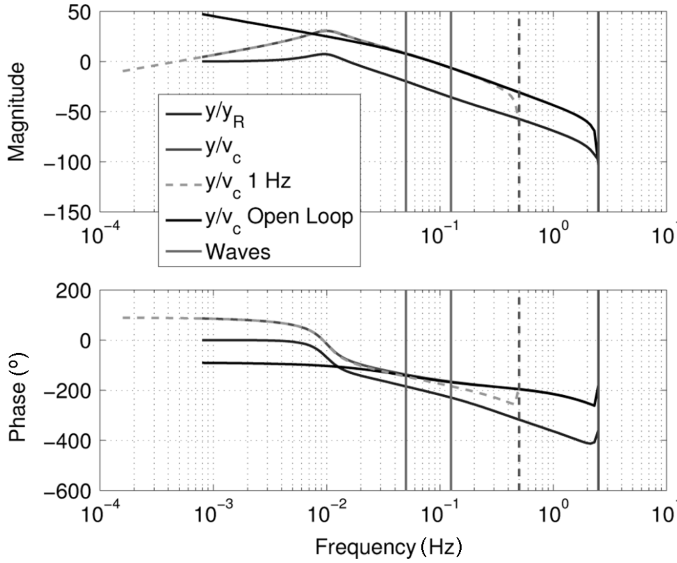

Fig. 10. Bode plot of cross-track docking control loops shown in Fig. 8.

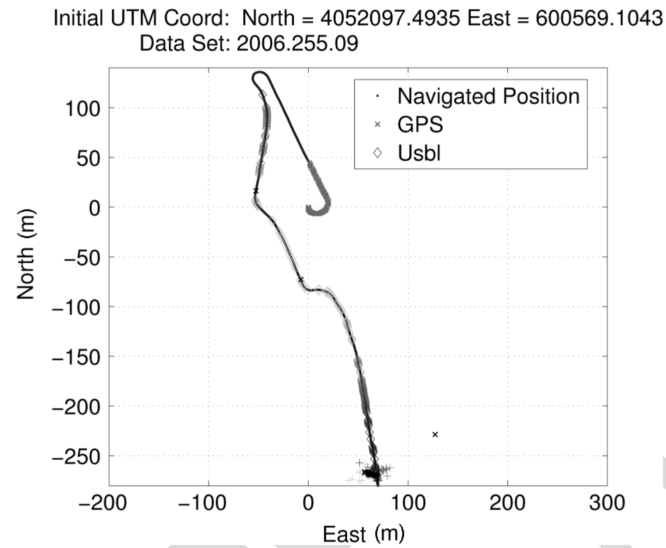

Fig. 11. Vehicle track during a docking trial. The + points are USBL measurements of the dock location. The diamonds show the vehicle's location when it took the measurement. Fig. 12 shows an enlargement of the point cluster at the bottom.

Please define ADPC] data taken during the docking trials showed that the wave period was 9.3 s with 3σ amplitude of about 30 cm/s. This data is summarized in Fig. 15.

The dashed green curves in Fig. 10 show the multirate transfer function with the outer USBL loop at 1 Hz, and the other loops at 5 Hz. The solid green curves show the best case for comparison, where the USBL loop is assumed to run at 5 Hz. The 1-Hz sampling does not appreciably degrade the performance. The dashed vertical red line shows the Nyquist frequency for the 1-Hz/5 Hz multirate system and the solid line for the 5-Hz monorate.

X. Sea-Trial Results

The MBARI team conducted the first at-sea homing trials on December 11, 2005, offshore Moss Landing, CA, which is north of Monterey. The test area had a flat bottom about 15 m deep, without any nearby obstructions or kelp beds. The transponder was moored about 5 m off the bottom. The vehicle was acquiring the transponder at distances exceeding 2 km and homing to within 50 cm. See [11] for details.

Docking was tested separately from homing, during summer and fall 2006 at the MISO, operated by Naval Postgraduate School (NPS, Monterey, CA) [16] and Associate Professor T. Stanton, who generously allowed MBARI full access to the facility. MISO is a cabled facility that provides power and Ethernet 600 m offshore, in 12 m of water. The shallow depth makes this site subject to 9–12-s short-period wave motion, as well as 12-h tidal currents. The observatory has an upward-looking ADCP, and NPS maintains an archive of water-current measurements stretching back for many years.

The docking flight pattern was a rectangle of 300×50 m^2, oriented with the long sides perpendicular to the shore. The approach to the dock at MISO was a corridor about 150 m wide, defined by kelp beds on either side, with the flight pattern running through this corridor. Docking tests began with the vehicle at the outer end of the rectangle, 300 m from the dock, where it would get a GPS fix. The vehicle then submerged and proceeded towards the outer marker waypoint, 200 m from the dock. At the outer marker, it slowed to 1.0 m/s and transitioned to the docking control state shown in Fig. 4, with the cross-track control loop shown in Fig. 8.

The USBL performed well during the 2005 homing trials, with little noise and few dropouts, leading us to conclude that little filtering was necessary. However, the noise environment at the MISO docking site was worse, due perhaps to the proximity of the shoreline, the surf, and nearby kelp beds.

The noisy USBL data at MISO was significant in that it was causing the vehicle to consistently miss the dock by 3–10 m. This led to the design of a moving-window median filter that proved to be very effective. The vehicle made the first controlled dock after implementing the filter and successfully docked on every attempt thereafter. There were four consecutive dockings.

A median filter can be effective for sonar applications because it rejects multipath, as long as there are fewer measurements corrupted by multipath than the uncorrupted ones.

Before median filtering, the USBL measurements were passed through simple outlier rejection tests. The data had to pass all of the following to be considered valid:

1) there must be a preset number of good consecutive samples;
2) the vehicle must not be turning too fast;
3) the measured bearing must not be too great.

These tests are not switched on until the vehicle is near enough to the transponder that the signal is strong.

The median filter then consists of taking the last 11 valid USBL measurements and computing the median of each axis individually. The navigation first converts the measurements to UTM***[AU: Please define UTM]*** locations, so that each measurement appears as a fixed location on a map, such as those in Figs. 11 and 12. Median filtering the eastings and

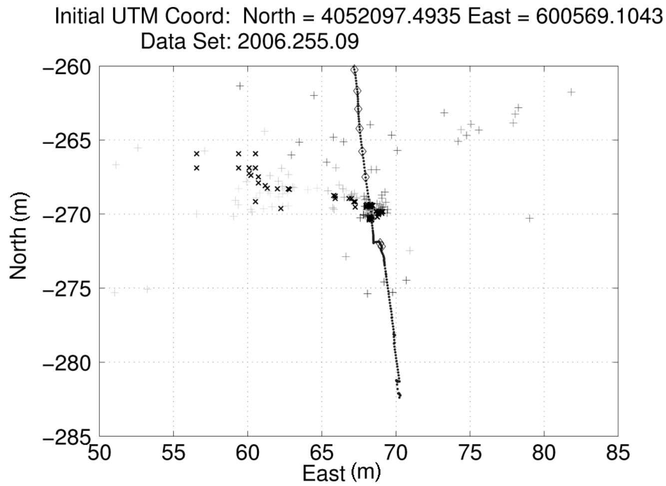

Fig. 12. Enlargement of the USBL dock hits. The $+$'s are raw data, and the x's are the filtered result. The colors of the $+$'s correspond to the diamonds in the preceding figure.

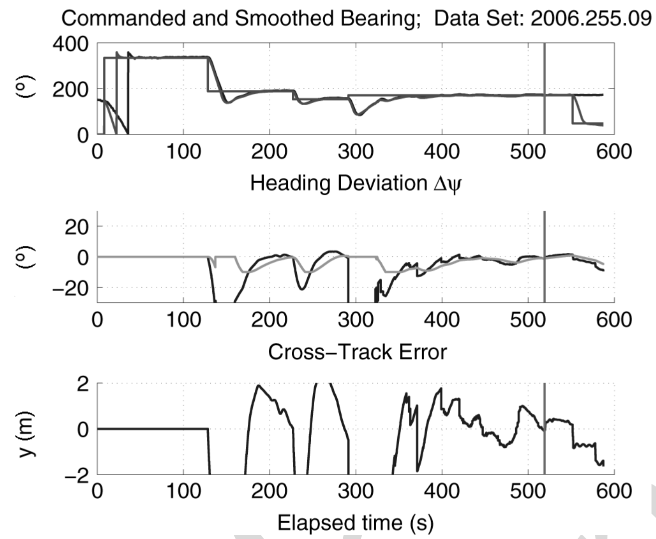

Fig. 13. Cross-track error, heading deviation, and heading during the docking event.

northings separately has the interesting effect of producing a location that is not the same as any of the measurements, yet it is contained within the largest cluster.

Fig. 11 shows the vehicle path, as seen from above, of the second docking mission. The axes are eastings and northings (UTM) in meters. The magenta points at the start, near (0,0), are GPS hits. The vehicle submerges, turns, and flies north to the first waypoint, then turns again to the south and passes through two more waypoints. The third waypoint is the outer marker where the vehicle transitions to docking control. The color-coded diamonds overlaying the path show the location of the vehicle at each USBL measurement. The color shows the distance from the transponder and corresponds to the color of the measured location indicated by a $+$. Black $\times$'s show the location of filtered points.

Fig. 12 shows a zoom of the dock location in Fig. 11. There is a distinct cluster of points about 8 m to the west of the dock, detected by the USBL when the vehicle was around 200 m out. The error is presumed to be due to a bounce (multipath). This cluster contains many valid hits. As the vehicle closes, however, this cluster is discarded by the moving window and the valid hits then cluster at the dock, precisely as desired.

Operators viewing the vehicle entering the dock on the video camera judged the position error to be between 5 and 10 cm, well under a vehicle diameter.

The jog after the third waypoint, at (0, -70), is caused by the initiation of the docking control loop. It turns the vehicle to the east to bring it onto the fixed flight path heading of $\psi_b = 171^\circ$. From that point in, the cross-track error is computed directly from USBL measurements, and not from propagated position.

The top strip of Fig. 13 shows yaw commands during the approach to the dock. The green line is commanded bearing to each of the three waypoints, followed by a flight path approach of 171°, beginning at 291 s. The approach bearing is labeled ψ_b in Fig. 8. The red line in Fig. 13 is the filtered heading command, and the blue is the measured. They correspond to $\psi_R = \Delta\psi_R + \psi_b$ and $\psi = \Delta\psi + \psi_b$, respectively. The commands to turn the vehicle from each waypoint to the next are clearly visible at 128 and 227 s, with ψ tracking as expected. The maneuver at 291 s is interesting, where ψ_R increases, but the vehicle commanded heading appears to turn in the opposite direction. This is because the docking controller has activated and must now slew the vehicle not only onto the specified bearing of $\psi_b = 171^\circ$, but must do so on the approach path. To do this, the docking controller must first turn the vehicle in the opposite direction to get onto the line, before turning back to the specified bearing.

The middle strip of Fig. 13 shows heading deviation $\Delta\psi$, which corresponds directly with the same symbol in Fig. 8. The green curve is the crab angle, commanded by the integrator. It is apparent that there is little cross current during this approach, since the crab angle approaches zero as the control reaches steady state just before each of the two waypoint changes.

The character of the blue $\Delta\psi$ curve changes when the waypoint control activates at 291 s. This is because the cross-track error was previously computed from the propagated position, determined from DVL-aided dead reckoning. After 291 s, the cross-track error is computed from the filtered USBL measurements and the compass. Several jumps in heading deviation are apparent between 320 and 450 s due to USBL noise.

The bottom strip shows the cross-track error. It is converging to under a meter after 400 s. Interestingly, the USBL apparently got some hits that took the vehicle almost a meter off track at 490 s, but then the measurements improved until the vehicle had zero measured cross-track error only about 4 s before contact. The measured error at the moment of contact, at 519 s, was 10 cm, slightly larger than what was apparent in the video.

There were three additional docking events, each appearing much like this one, indicating that the docking control is repeatable, at least in the cross-current conditions shown in Fig. 15.

Depth control is unchanged from the standard algorithm as described in [9]. The vehicle flew at 12-m depth during its final approach, until about 50 m out, where it transitioned to a 3-m altitude track. The dock is located on a slight slope and is 3 m high in 12 m of water.

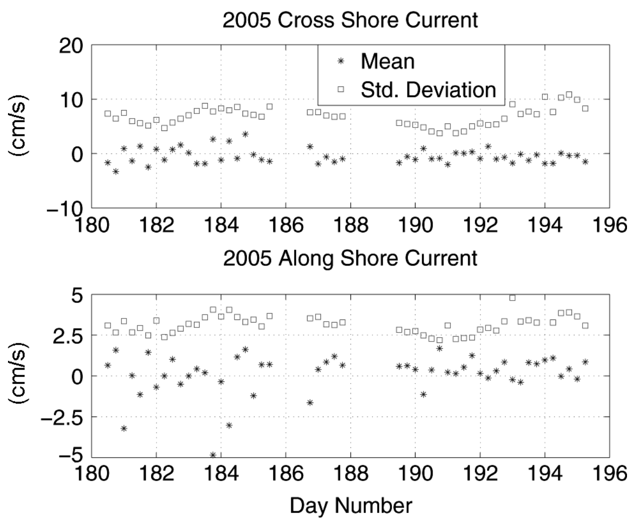

Fig. 14. Six-hour current statistics at 1.8-m altitude. Ten-second wave motion is averaged out.

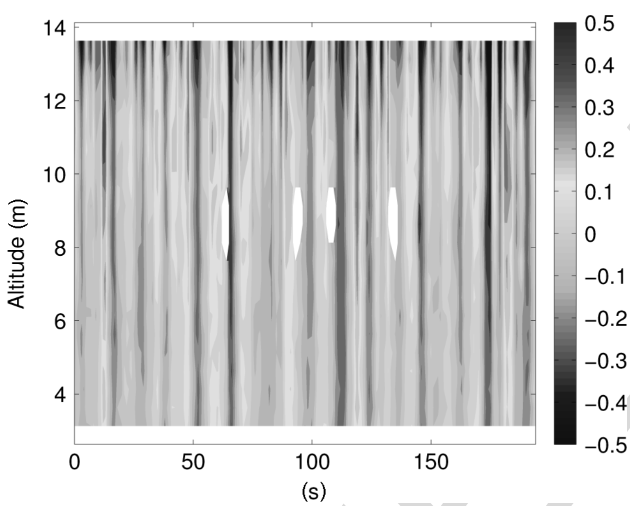

Fig. 15. Along-shore current as a function of altitude at MISO on the moment of the docking event in Figs. 11–13, September 12, 2006 (day 255), 19:36:00 Z. The colorbar shows meters per second.

XI. Dock Test Environment

Fig. 14 shows statistics of cross-shore and along-shore tidal currents at the MISO docking test site during July and August 2005, which is a representative period for the docking trials. The measurements are at 1.8-m altitude. The along-shore current is of primary concern because it is perpendicular to the approach path and will tend to carry the vehicle off track. The vehicle approach altitude was 3 m, where the current was expected to be larger, and so the design had to allow for currents greater than shown.

Blue points are the mean current over a 6-h period, which shows the tidal component with wave motion averaged out. The sampling period was between 1 and 2 s. Tidal currents act as a constant during a docking approach because an approach takes only a few minutes.

The standard deviation of the along-shore tidal component is 3.8 cm/s, with a maximum surpassing 5 cm/s. The constant-current design specification was consequently taken to be 25 cm/s, keeping in mind that the currents tend to be faster further above the sea bed, and allowing a margin. High-frequency ADCP data, such as that shown in Fig. 15, was not obtained in time for the control design, and so the design is based primarily on the data in Fig. 14.

Fig. 15 shows a 3-min segment of the full 1-s data set of along-shore current measurements, taken on the day that the AUV docked. At meters altitude, the tidal (average) current was 2.0 cm/s to the north, with a 9.3-s wave component, with standard amplitude deviation of $\sigma = 9.4$ cm/s.

The figure shows that the short-period wave current tends to increase with altitude, justifying a design margin for current greater than what was measured at 1.8 m in Fig. 14.

XII. Conclusion

A prototype AUV docking system has been designed, built, and tested at sea. The dock was attached to the MISO cabled observatory in southern Monterey Bay, and used to support docking operations with a Dorado 54-cm-diameter (21 in) AUV. All of the capabilities required for a docking capability for seafloor observatories have been demonstrated, including the following:

1) homing and capture of the AUV in the docking station;
2) establishing an Ethernet connection between the vehicle and the dock using a short-range radio frequency communication system;
3) complete interactivity with the vehicle including recovering mission data to shore, downloading new missions to the vehicle, and even adding new code to the vehicle and compiling *in situ*;
4) inductive transmitting power to the vehicle;
5) charging vehicle batteries from observatory power;
6) turning the vehicle off, and then waking it up from the dock;
7) undocking the vehicle from the dock and commencing missions.

Appendix

See Tables II–VI.

TABLE II
General Parameters and Mass Properties in (1)–(6) for the Homing Control

m	640.3	kg	Mass
I_{zz}	475.0	kg-m^2	Inertia
x_G	0.119	m	CG offset
x_R	-1.79	m	Dist. to rudder
x_A	-1.03	m	Dist. to antenna
U	1.54	m/s	Speed
T_p	52	N	Thrust
ρ	1025	kg/m^2	Density of seawater

TABLE III
STABILITY DERIVATIVE VALUES IN (1)–(6)

$Y_{\dot{v}}$	-595.0	kg	Added mass
$Y_{\dot{r}}$	-57.91	kg	
$N_{\dot{v}}$	-57.91	kg-m^2	Added Inertia
$N_{\dot{r}}$	-381.4	kg-m^2	
Y_v	-106.0	kg/m	Force deriv.
Y_r	37.90	kg	
N_v	-494.9	kg	Munk moment
N_r	-288.1	kg-m	Torque deriv.

TABLE IV
HYDRODYNAMIC VALUES FOR RING WING IN (1)–(6)

d_R	0.381	m	Diameter
c_R	0.127	m	Chord
$C_{L\alpha}$	4.80	radians^{-1}	Coef. of lift slope
C_{Do}	0.012	none	Coef. of drag

TABLE V
HYDRODYNAMIC VALUES FOR RING-WING STRUTS IN (1)–(6)

b_S	0.127	m	Span
$\bar{c}_S$	0.043	m	Chord
$C_{SL\alpha}$	6.28	radians^{-1}	Coef. of lift slope
C_{SDo}	0.012	none	Coef. of drag

TABLE VI
HYDRODYNAMIC VALUES FOR GPS/RF ANTENNA FIN IN (1)–(6)

b_F	0.254	m	Span
$\bar{c}_F$	0.0762	m	Chord
$C_{FL\alpha}$	4.4	radians^{-1}	Coef. of lift slope
C_{FDo}	0.005	none	Coef. of drag

TABLE VII
HOMING CONTROL GAINS IN FIG. 6

K_p	0.4	none	Position gain
K_r	2.0	seconds	Rate gain
K_v	0.0	radians/meter/second	Lateral speed gain
K_I	0.02	seconds^{-1}	Integral gain
T	0.2	seconds	Sampling period

TABLE VIII
DOCKING CONTROL GAINS IN FIG. 8

K_p	1.0	none	Position gain
K_r	2.0	seconds	Rate gain
K_v	0.0	radians/meter/second	Lateral speed gain
K_{wp}	0.05	radians/meter	Wpnt. posn. gain
K_{Iwp}	0.003	radians/second/meter	Wpnt. intgrl. gain
T	0.2	seconds	Sampling period
a	1/2.5	seconds^{-1}	Filt. nat. freq.
K	$1 - e^{aT}$	none	Filt. gain

ACKNOWLEDGMENT

This work would not have been possible without the sustained effort of the entire MBARI Docking team, including J. Erickson, T. Hoover and F. Shane, as well as important contributions from H. Thomas, R. Henthorn, J. Connor (MBARI), S. Rock (Stanford University), and others. The authors would particularly like to thank T. Stanton (Naval Postgraduate School) for providing the ADCP data in Figs. 14 and 15, and also allowing them full and unrestricted access and use of the Monterey Inner Shelf Observatory, which provided the undersea power and data cable, and infrastructure required to support the dock.

REFERENCES

[1] J. Evans, P. Redmond, C. Plakas, K. Hamilton, and D. Lane, "Autonomous docking for intervention-style AUVs using sonar and video-based real-time 3D pose estimation," in *Proc. MTS/IEEE OCEANS Conf.*, San Diego, CA, Sep. 2003, pp. 2201–2210.

[2] T. Fukasawa, T. Noguchi, T. Kawasaki, and M. Baino, "Marine bird—A new experimental AUV with underwater docking and recharging system," in *Proc. MTS/IEEE OCEANS Conf.*, San Diego, CA, Sep. 2003, pp. 2195–2200.

[3] H. Singh, J. G. Bellingham, F. Hover, S. Lerner, B. A. Moran, K. Heydt, and D. Yoerger, "Docking for an autonomous ocean sampling network," *IEEE J. Ocean. Eng.*, vol. 26, no. 4, pp. 498–513, Oct. 2001.

[4] B. Allen, T. Austin, N. Forrester, R. Goldsborough, A. Kukulya, G. Packard, M. Purcell, and R. Stokey, "Autonomous docking demonstrations with enhanced REMUS technology," in *Proc. MTS/IEEE OCEANS Conf.*, Boston, MA, Sep. 2006, pp. 1–6, doi: 10.1109/OCEANS.2006.306952.

[5] R. Stokey, B. Allen, T. Austin, R. Goldsborough, N. Forrester, M. Purcell, and C. V. Alt, "Enabling technology for REMUS docking: An integral component of an autonomous ocean sampling network," *IEEE J. Ocean. Eng.*, vol. 26, no. 4, pp. 487–497, Oct. 2001.

[6] S. Cowen, S. Briest, and J. Dombrowski, "Underwater docking of an autonomous undersea vehicle using optical terminal guidance," in *Proc. MTS/IEEE OCEANS Conf.*, Halifax, NS, Canada, Oct. 1997, pp. 1143–1147.

[7] P. M. Lee, B. H. Jeon, and S. M. Kim, "Visual servoing for underwater docking of an autonomous vehicle with one camera," in *Proc. MTS/IEEE OCEANS Conf.*, San Diego, CA, Sep. 2003, pp. 2195–2200.

[8] ***[AU: Please provide city and state of the institution]***M. Gertler, "Resistance experiments on a systematic series of streamlined bodies of revolution—For application to the design of high-speed submarines," Navy Department, The David Taylor Model Basin, Rep. C-297, Apr. 1950.

[9] ***[AU: Please provide page range]***R. S. McEwen and K. Streitlien, "Modeling and control of a variable-length AUV," in *Proc. 12th Int. Symp. Unmanned Untethered Submersible Technol.*, Durham, NH, Aug. 2001.

[10] M. D. Feezor, F. Y. Sorrel, P. R. Blankenship, and J. G. Bellingham, "Autonomous underwater vehicle homing/docking via electromagnetic guidance," *IEEE J. Ocean. Eng.*, vol. 26, no. 4, pp. 515–521, Oct. 2001.

[11] ***[AU: Please provide page range]***J. G. Bellingham, R. S. McEwen, and B. W. Hobson, "The development of a docking station for a regional cabled observatory," in *Proc. 4th Int. Workshop Scientific Use of Submarine Cables*, Dublin, Ireland, Feb. 2006.

[12] ***[AU: Please provide volume and issue]***R. Coulson, J. Lambiotte, and E. An, "A modular docking system for 12.75-inch class AUVs," *Sea Technol.*, pp. 49–54, Apr. 2005.

[13] ***[AU: Please provide city and state of the institution]***M. Gertler and G. Hagen, "Standard equations of motion for submarine simulation," David W. Taylor Naval Ship Research and Development Center, Rep. 2510, 1967.

[14] T. I. Fossen, *Guidance and Control of Ocean Vehicles*. New York: Wiley, 1994.

[15] M. Guelman, "A qualitative study of proportional navigation," *IEEE Trans. Aerosp. Electron. Syst.*, vol. AES-7, no. 4, pp. 637–643, Jul. 1971.

[16] T. Stanton, Monterey Inner Shelf Observatory Web Page Moss Landing, CA [Online]. Available: http://www.oc.nps.navy.mil/~stanton/miso

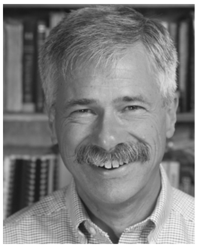

Robert S. McEwen (M'99) was born in Cleveland, OH, in 1955. He received the B.S. degree in electrical engineering from Purdue University, West Lafayette, IN, in 1978, the M.S. degree in electrical engineering from the University of Illinois, Chicago, in 1982, and the M.S. degree in mechanical engineering from Stanford University, Stanford, CA, in 1988. His specialization was dnamics and control.

He worked at Lockheed Corporation from 1982 to 1988 on spacecraft attitude control and navigation. From 1988 to 1997, he worked at Integrated Systems Incorporated on a variety of control-system related projects, from automotive power steering to spacecraft control. He was the Principal Engineer for the control system of the Miniature Sensor Technology Integration (MSTI) spacecraft, which operated successfully in orbit for over a year, exceeding its design life. Since 1998, he has worked primarily on autonomous underwater vehicle (AUV) guidance, navigation, and control systems for the Monterey Bay Aquarium Research Institute, Moss Landing, CA.

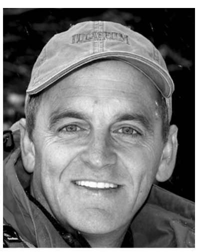

Brett W. Hobson (M'98) received the B.S. degree in mechanical engineering from California State University, San Francisco, in 1989.

Currently, he is working with the Platforms Group within the R&D Department, Monterey Bay Aquarium Research Institute (MBARI), Moss Landing, CA. Before joining MBARI, he helped start Nekton Research, a Navy R&D contractor specializing in small underwater vehicles. He started designing, building, and operating undersea systems at Deep Ocean Engineering and Deep Sea Discoveries.

Mr. Hobson is a member of the Marine Technology Society and American Geophysical Union.

Lance R. McBride (M'96) received the B.S. degree in electrical engineering from Walla Walla College, College Place, WA, in 1996.

He has worked in the fields of network engineering, particle acceleration, high-speed video electronics, and oceanographic equipment. He is currently consulting as an Electrical Engineer, and was formerly an Electrical Engineer with the Research and Development Department, Monterey Bay Aquarium Research Institute (MBARI), Moss Landing, CA. His professional interests include low-power electronics, imaging systems, human interface technology, and circuit card design. He has authored and coauthored numerous publications for the IEEE Oceanic Engineering Society and other publications.

Mr. McBride has been a member of the Association for Computing Machinery (ACM) and was a licensed Microsoft Certified Systems Engineer (MCSE). He was the president of his IEEE student body during his senior year at Walla Walla College, and was awarded third place for his IEEE student entry at the Columbia Basin Technical Conference and Trade Show in 1996. He has been a Registered Professional Engineer in the State of California since 2006.

James G. Bellingham (M'XX)***[AU: Please provide membership year. The information was not found in the IEEE database. Please provide educational background]***

Currently, he is the Chief Technologist at the Monterey Bay Aquarium Research Institute (MBARI), Moss Landing, CA. His personal research activity revolves around the development and use of autonomous underwater vehicles (AUVs). In the process of developing these vehicles, he spent considerable time at sea, leading over 20 AUV expeditions. He leads the Autonomous Ocean Sampling Network (AOSN) program at MBARI, which uses fleets of autonomous vehicles to adapt to and observe rapidly changing oceanographic processes.